A DCL3 dicing code within Pol IV-RDR2 transcripts diversifies the siRNA pool guiding RNA-directed DNA methylation

Andrew Loffer[1], Jasleen Singh[1], Akihito Fukudome[1,2], Vibhor Mishra[1,2], Feng Wang[1,2] and Craig S. Pikaard[1,2,*]

[1]Department of Biology and Department of Molecular and Cellular Biochemistry, Indiana University, Bloomington, IN, USA

[2]Howard Hughes Medical Institute, Indiana University, Bloomington, IN, USA

[*]Correspondence: cpikaard@indiana.edu;

Summary

In plants, selfish genetic elements including retrotransposons and DNA viruses are transcriptionally silenced by RNA-directed DNA methylation. Guiding the process are short interfering RNAs (siRNAs) cut by DICER-LIKE 3 (DCL3) from double-stranded precursors of ~30 bp synthesized by NUCLEAR RNA POLYMERASE IV (Pol IV) and RNA-DEPENDENT RNA POLYMERASE 2 (RDR2). We show that Pol IV initiating nucleotide choice, RDR2 initiation 1-2 nt internal to Pol IV transcript ends and RDR2 terminal transferase activity collectively yield a code that influences which end of the precursor is diced and whether 24 or 23 nt siRNAs are generated from the Pol IV or RDR2-transcribed strands. By diversifying the size, sequence, and strand polarity of siRNAs derived from a given precursor, alternative patterns of DCL3 dicing allow maximal siRNA coverage at methylated target loci.

Keywords: Dicer endonuclease, DICER-LIKE 3, siRNA biogenesis, NUCLEAR RNA POLYMERASE IV, RNA-DEPENDENT RNA POLYMERASE 2, gene silencing, RNA silencing

Introduction

In eukaryotes, short interfering RNAs (siRNAs) are used to suppress DNA transcription or mRNA translation, thereby playing important roles in gene regulation (Ipsaro and Joshua-Tor, 2015; Martienssen and Moazed, 2015; Shabalina and Koonin, 2008). Plant siRNAs range in size from 21nt to 24 nt, with DCL3-dependent 23 and 24 nt siRNAs (Henderson et al., 2006; Xie et al., 2004) accounting for ~90% of the total siRNA pool (Kasschau et al., 2007; Mosher et al., 2008; Zhang et al., 2007). The 24 nt siRNAs stably associate with one of several Argonaute family proteins, primarily ARGONAUTE 4 (AGO4) (Zilberman et al., 2003), and guide resulting complexes to target loci via basepairing interactions with long noncoding RNAs synthesized by multisubunit NUCLEAR RNA POLYMERASE V (Figure 1A) (Wierzbicki et al., 2008; Wierzbicki et al., 2009). Protein-protein interactions between AGO4 and the C-terminal domain of the Pol V largest subunit, or Pol V-associated protein SPT5L, also contribute to AGO4 localization at target loci (El-Shami et al., 2007; Lahmy et al., 2016). Subsequent recruitment of the *de novo* DNA methyltransferase, DRM2 (Cao and Jacobsen, 2002; Zhong et al., 2014) and other chromatin modifying enzymes then leads to the establishment of repressive chromatin environments that inhibit promoter-dependent transcription by DNA-dependent RNA Polymerases I, II or III (Matzke and Mosher, 2014; Wendte and Pikaard, 2017). In this way, RNA-directed DNA methylation (RdDM) facilitates transcriptional silencing at thousands of loci throughout plant genomes.

Biogenesis of siRNAs involved in RdDM begins with DNA transcription by Pol IV, a 12-subunit DNA-dependent RNA polymerase that evolved as a specialized form of Pol II (Ream et al., 2009). Pol IV associates with RDR2 (Haag et al., 2012; Law et al., 2011) via direct physical interaction (Mishra et al., 2021) to form a multi-functional enzyme complex. The transcription reactions of Pol IV and RDR2 are tightly coupled (Singh et al., 2019) to produce double-stranded RNAs (dsRNAs) of ~25-40 bp (Blevins et al., 2015; Yang et al., 2016; Ye et al., 2016; Zhai et al., 2015). By incubating purified Pol IV, RDR2 and DCL3 with single-stranded bacteriophage M13 template DNA and nucleoside triphosphates, 23 and 24 nt siRNA biogenesis can be recapitulated *in vitro*, indicating that no other activities are needed (Singh *et al.*, 2019).

Importantly, when AGO4 is immunoprecipitated, associated siRNAs are almost entirely 24 nt (Havecker et al., 2010; Mi et al., 2008), making the significance of 23 nt siRNAs unclear. We have proposed that when paired with 24 nt siRNAs, the 23 nt RNAs help specify the AGO4-

association of the 24 nt siRNA strand (Singh et al, 2019), a hypothesis now supported by experimental evidence (Wang and Pikaard; manuscript in preparation).

In this study, we investigated the rules of DCL3 dicing, revealing how Pol IV and RDR2-encoded cues program DCL3 dicing patterns and account for the biogenesis of either 23 or 24 nt siRNAs. We show that DCL3 preferentially binds dsRNAs with 3' overhangs, that overhangs are present at both ends of Pol IV-RDR2 dsRNA transcripts to facilitate dicing from either end, and that two distinct activities of RDR2 account for the 3' overhangs at both ends of the dsRNAs. The choice of nucleotide incorporated at the 5' terminus of Pol IV transcripts also affects DCL3 interaction, and which end of the dsRNA is diced. Our evidence indicates that DCL3 measures only one strand of its substrate dsRNAs, with RNase III domain B cutting the measured strand to produce 24 nt siRNAs and domain A cutting the non-measured strand to produce either 23 nt or 24 nt siRNAs. Collectively, our experiments reveal a code comprised of sequence and structural features that are intrinsic to paired Pol IV- RDR2 transcripts and program alternative DCL3 dicing patterns thereby diversifying siRNA size, sequence and polarity.

Results

DCL3 preferentially dices double-stranded RNAs with 3' overhangs

Previously, we showed that an untemplated nucleotide is often present at the 3' ends of RDR2 transcripts and persists among 23 nt, but not 24 nt siRNAs, derived from the RDR2-transcribed strands of precursor dsRNAs (Singh and Pikaard, 2019). We also showed that RDR2 has terminal transferase activity, which can account for untemplated nucleotide addition at RDR2 transcript 3' ends (Blevins *et al.*, 2015). These observations led to a model (Singh *et al.*, 2019; Singh and Pikaard, 2019), shown in Figure 1B, in which we proposed that DCL3 interacts with basepaired Pol IV-RDR2-transcripts and measures 24 nt from the 5' terminus of the Pol IV strand (shown as the top strand in Figure 1B and throughout this paper), cuts the Pol IV strand at that position, and makes a second cut of the RDR2 strand that is offset by 2nt from the cut made in the Pol IV strand. Because of the untemplated nucleotide added to the 3' end of the RDR2 strand, an asymmetric 24/23 nt siRNA duplex would be the predicted dicing product (Singh *et al.*, 2019).

To test whether DCL3 can, in fact, carry out the hypothetical reaction depicted in Figure 1B, recombinant DCL3 produced in insect cells was purified to near-homogeneity (Figure 1-figure supplement 1-panel A) and incubated with a dsRNA generated by annealing 37 and 38 nt RNAs (see Supplementary Table 1 for RNA strand sequences). This dsRNA has a 3' overhang of 1 nt on the left side, as drawn in Figure 1C, to mimic the overhang attributable to RDR2's terminal transferase activity. DCL3 cuts the 37/38 nt dsRNA to yield 23 and 24 nt products (Figure 1C, lanes 1 and 5) as predicted by the model. Similarly, DCL3 cuts a dsRNA with a 2 nt overhang, formed by annealing 37 and 39 nt RNAs, to generate two 24 nt RNAs (Figure 1C, lanes 2 and 6). These results are consistent with the hypothesis that DCL3 measures and cuts 24 nt from the 5' end of the top strand, and makes an offset cut of the bottom strand to leave a 2 nt 3' overhang, as expected from prior studies (Nagano et al., 2014; Takeshita et al., 2007; Zhang et al., 2004). The results also suggest that the length of the bottom strand can vary, indicating that its 3' end is not anchored at a fixed position by DCL3.

Given a dsRNA substrate with two blunt ends, DCL3 generates dicing products of diverse size, including 21, 22, 24 and 25 nt RNAs (Figure 1C, compare lanes 3 and 7). Gel-mobilities depend on RNA sequence, thus RNAs of the same length, but from opposite strands of the dsRNA, differ in mobility as is apparent in Figure 1C. Importantly, 21, 22, and 25 nt dicing products are not observed at significant levels among siRNAs produced *in vitro* by Pol IV, RDR2 and DCL3 (Singh *et al.*, 2019), nor have RNAs of these sizes been attributed to DCL3 activity based on analysis of *dcl3* mutants *in vivo* (Henderson *et al.*, 2006; Xie *et al.*, 2004). These considerations, combined with the results of Figure 1C, indicate that dsRNAs with 3' overhangs, not blunt ends, best account for the 23 and 24 nt siRNAs generated by DCL3.

To more definitively test whether DCL3 prefers 3' overhangs over blunt ends, we performed DCL3 cleavage assays using dsRNAs that have a 3' overhang on the left side and a blunt end on the right side, with either the top strand or bottom strand end-labeled with ^{32}P (Figure 1D). If the 3' overhanging end is preferred by DCL3, a 24 nt ^{32}P-labeled dicing product is expected from the ^{32}P-labeled top strand and a 16 nt product is expected from the ^{32}P-labeled bottom strand. This is what is observed, with dsRNA substrates that have 3' overhangs of 1 or 2 nt yielding nearly identical products (Figure 1D, compare lanes 1-4 to lanes 5-8) and reaction time-courses (Figure 1-figure supplement 1-panel B). In contrast, if DCL3 is incubated with a dsRNA with two blunt ends, DCL3 dices from both ends, generating 16 and 24 nt products from

both strands (Figure 1E). Collectively, the results of Figure 1 show that DCL3 will cut dsRNAs with 3' overhanging ends or blunt ends but prefers 3' overhanging ends.

DCL3 measures 24 nt from the recessed 5' end of dsRNAs with 3' overhangs

Experiments testing the dicing of dsRNAs formed by annealing RNA strands ranging in size from 22-25 nt yielded additional evidence that DCL3 measures only one strand of its dsRNA substrates (Figure 2). Using a duplex whose top strand was 24 nt and whose bottom strand was 25 nt, thus generating a 1 nt 3' overhang on the left side, the 24 nt top strand was not cut by DCL3, but the bottom strand was trimmed by 2 nt to yield a 23 nt product (Figure 2A). We next tested a duplex with two blunt ends, formed by annealing two 24 nt RNAs (Figure 2B; note that these 24 nt RNAs display slightly different gel mobilities). Dicing by DCL3 occurred from the left or right sides, due to the absence of a 3' overhang to bias dicing to one side. In each case, one 24 nt strand was uncut whereas the paired strand was trimmed to 22 nt RNA (Figure 2B, lane 3; note that the alternative 22 nt RNAs also have different gel mobilities).

An informative dicing pattern was observed for a duplex formed by annealing a 23 nt top strand with a 24 nt bottom strand and having a 1 nt 3' overhang on the left side. Dicing of this substrate resulted in the 24 nt bottom strand being cut, but trimmed by only 1 nt (Figure 2B, lanes 4 and 5). This indicates that DCL3's measurement of an interval equivalent to 24 nt is a consequence of interaction with the recessed 5' end of the top strand. The bottom strand was cut at a position offset by 2 nt from where the 24th nucleotide would have been present in the top strand had the top strand been long enough.

Next, we annealed a 24 nt top strand and a 23 nt bottom strand to generate a duplex with a 1 nt 3' overhang on the left side and a 2 nt 3' overhang on the right side (Figure 2C), which mimics the dicing product proposed in Figure 1B and verified in Figure 1C. DCL3 does not cut either stand of this duplex RNA (Figure 2C, compare lanes 2 and 3). This suggests that the asymmetric 24/23 nt dsRNA duplex fits into the enzyme with the RNase domains aligned with the pre-existing ends of the RNA strands. As a result, no cutting occurs. A 24/24 nt duplex having 2 nt 3' overhangs at both ends was also not cut by DCL3 (Figure 2C, compare lanes 4 and 5). These results indicate that DCL3 dicing products are not substrates for further dicing.

Unlike 24/23 and 24/24 dicing products that are not diced further, duplexes formed by annealing 23 and 22 nt RNA strands, in various permutations, yielded a ladder of digestion

products as short as 17 nt (Figure 2D). This suggests that dsRNAs whose strands are shorter than typical DCL3 dicing products do not fit into the enzyme in a way that fixes their position, allowing for cutting at variable positions. The results also raise the possibility that DCL3 could play a role in the cleavage and turnover of dsRNAs smaller than its dicing products *in vivo*.

Strand-cutting specificities of DCL3's RNase III domains

To determine how DCL3 is oriented on its dsRNA substrates, we mutated RNase III domains A and B by converting glutamates E1146 and/or E1329 to glutamines (Figure 3A). We then tested the cutting of a dsRNA formed by annealing 26 and 27 nt RNAs, with a 1 nt 3' overhang on the left side (Figure 3B). DCL3 with wild type, unmutated RNase domains cut both strands of the dsRNA to yield 24 nt and 23 nt siRNAs (compare lanes 5 and 6). Mutating both RNase III domains abolished dicing (compare lane 5 and 7). Mutating RNase III domain A, while leaving domain B unchanged, resulted in top strand (26 nt) cutting to 24 nt, but no bottom strand (27 nt) cutting (lane 8). Conversely, mutating domain B, but leaving domain A unchanged, allowed bottom strand cutting, to 23 nt (lane 9). Repeating these experiments using a dsRNA substrate with a 2 nt overhang, instead of a 1 nt overhang, yielded equivalent results, the only difference being the generation of a 24 nt product from the bottom strand due to the additional overhanging nucleotide (Figure 3-figure supplement 1). Collectively, these results indicate that the PAZ domain binds the recessed 5' end of the top RNA strand, opposite the 3' overhang of the bottom strand, and cuts that strand using RNase III domain B at a distance equivalent to 24 nt. The paired strand is cut by RNase III domain A, with the 3' overhanging end of this strand not anchored at a fixed distance, allowing its diced products to vary in length (Figure 3C).

DCL3 substrate recognition is influenced by 5' terminal nucleotide and phosphorylation status

Pol IV transcripts tend to have a purine at their 5' ends (as denoted in Figure 1B), with A being more prevalent than G (Singh *et al.*, 2019). However, pyrimidines can also serve as the initiating nucleotide, with C used more frequently than U (Singh et al., 2019). We thus tested whether the 5'-terminal nucleotide affects DCL3 dicing using dsRNA substrates with a 1 nt 3' overhang on the left side, a blunt-end on the right side, and a top strand that begins with A, G, C

or U (Figure 4A). This experiment revealed that DCL3 cleaves dsRNA substrates whose top strands begin with 5' A or U (lanes 5-10) more efficiently than those beginning with C or G (lanes 11-16), in agreement with prior results comparing cell-free lysates of wild-type and *dcl3* mutant plants (Nagano *et al.*, 2014). The fact that A or U allow for similar dicing efficiency suggests that an AU or UA pair is preferred over a GC or CG pair at the precursor's terminus, which may have a structural basis.

We next tested whether DCL3 is affected by the nucleotide at the 3' overhanging position of the bottom strand (Figure 4B). No significant difference in cleavage efficiency was observed for bottom strands having A, U, C or G as the overhanging nucleotide, indicating that although the presence of 3' overhang is important for dicing (Figure 1D), the identity of the overhanging nucleotide is unimportant.

The 5' terminal nucleotide of a nascent transcript is expected to possess a 5' triphosphate group, and biochemical evidence indicates that this is true for RDR2 transcripts (Singh *et al.*, 2019). However, Pol IV-dependent transcripts generated *in vivo* or *in vitro* can be cloned via ligation reactions that require a 5' monophosphate, without prior enzymatic treatments (Blevins *et al.*, 2015; Li et al., 2015; Singh *et al.*, 2019; Zhai *et al.*, 2015), suggesting the possibility of an intrinsic or associated pyrophosphatase activity. We tested whether monophosphate or triphosphate groups at the 5' end of a dsRNA substrate affects DCL3 dicing. For this experiment, dsRNA substrates had 1 nt 3' overhangs (uridines in each case) and 5' adenosines at each end (Figure 4C), making both ends similarly conducive to dicing. The top strand in all cases was 5' end-labeled with a ^{32}P monophosphate. The 5' end of the bottom strand had either a triphosphate, a monophosphate, or a hydroxyl group. Dicing initiated by measuring 24 nt from the 5' end of the top strand yields a 24 nt labeled product, whereas dicing measured 24 nt from the 5' end of the bottom strand yields a 16 nt labeled product. The ratio of 24 versus 16 nt products thus provides a way to assess the relative affinity of DCL3 for dicing the alternative ends of the substrate dsRNA. This experiment revealed that if the bottom strand has a 5' hydroxyl group, a strong 24 nt signal and weak 16 nt signal (barely above background levels) was observed (Figure 4C, lane 4). This indicates that DCL3 preferentially engaged the left side of the dsRNA substrate, which has a 5' monophosphate, and disfavored the right side, which has a 5' hydroxyl. However, if the bottom strand also has a 5' monophosphate (lane 5), or a triphosphate (lane 6), more right-

side dicing occurs suggesting that monophosphates or triphosphates are similarly conducive to DCL3 engagement.

DCL3 dicing does not require ATP

Drosophila melanogaster Dicer-2 displays ATP-dependent activity for substrates with blunt-ends, but not overhanging ends (Sinha et al., 2018). Moreover, experiments comparing cell-free lysates of wild-type versus *dcl3* mutant Arabidopsis plants suggested that binding, but not hydrolysis, of ATP is needed for DCL3 activity (Nagano *et al.*, 2014). We thus tested whether dicing by purified DCL3 is ATP-dependent using a dsRNA substrate formed by annealing a 37 nt top strand RNA, 5' end-labeled with ^{32}P, to unlabeled 37, 38 or 39 nt bottom strands, thereby generating dsRNAs with either two blunt ends or with a 1 or 2 nt overhang on the left side and a blunt end on the right side (Figure 5). DCL3 dicing from the left side of these substrates generates a 24 nt labeled product. In reactions containing 0 mM ATP, 5 mM ATP, or 5 mM ATP-γ-S, a non-hydrolysable form of ATP, no differences in DCL3 dicing activity were observed (lanes 2-4, 6-9, and 10-12) for any of the substrates. We conclude that DCL3 does not require either ATP binding or ATP hydrolysis for dicing.

Overhangs at both ends of DCL3 substrates explain 24 and 23 nt siRNA biogenesis from both strands

The model in Figure 1B, supported by the experiments of Figures 1-3, accounts for how DCL3 can produce a diced duplex consisting of a 23 nt siRNA derived from the RDR2-transcribed strand and a 24 nt siRNA derived from the Pol IV strand. However, the model does not account for our prior RNA-seq data that showed that 23 and 24 nt siRNAs are generated from both strands (Singh *et al.*, 2019). This led us to construct an expanded model (Figure 6A) in which DCL3's ability to dice from either the left or right side of a duplex and DCL3's penchant for 3' overhangs were considered. Scenario 1 of Figure 6A is the scenario of Figure 1B, with the left-side 3' overhang generated by RDR2's addition of an untemplated nucleotide (N). In scenarios 2 and 3, we hypothesized that 3' overhangs on the right side could occur if RDR2 initiates transcription 1 or 2 nt internal to the 3' end of the Pol IV transcript.

To experimentally test for single-stranded overhangs at the ends of Pol IV and RDR2 transcripts, we conducted transcription reactions as in Singh et al., 2019, using ^{32}P to specifically

label either the Pol IV or RDR2 strands of their dsRNA products. We then treated the transcripts with S1 nuclease, which digests single-stranded nucleic acids (Figure 6B). For these experiments, Pol IV transcription was initiated using an RNA primer hybridized to a T-less (lacking thymidines) DNA template (see diagram in Figure 6B and Supplementary Table 2 for oligonucleotide sequences). Downstream of the primer used to initiate transcription, a non-template DNA oligonucleotide is annealed to the template DNA to induce Pol IV arrest and RDR2 engagement of the Pol IV transcript's 3' end, enabling synthesis of the RDR2-transcribed strand (Singh *et al.*, 2019). By 5' end-labeling the RNA primer, only first-strand RNAs synthesized by Pol IV are labeled and detected. Conversely, by using an unlabeled RNA primer and including alpha-labeled ^{32}P-ATP in the reactions, second-strand RNAs synthesized by RDR2 are specifically labeled. Note that because As are not present in first-strand RNAs generated by Pol IV transcription of a T-less DNA template, first strands are not labeled.

Treatment of transcription reaction products with increasing amounts of S1 nuclease resulted in a progressive 1-2 nt shortening of labeled Pol IV transcripts (Figure 6B, lanes 1-4). Because the ^{32}P label is at the 5' end of these Pol IV transcripts, S1 trimming must be occurring at their 3' ends. Body-labeled RDR2 transcripts were shortened by 1 nt upon digestion with S1 nuclease (Figure 6B, lanes 5-8), a result consistent with the removal of the single untemplated nucleotide added to the 3' end of RDR2 transcripts. Collectively, the data of Figure 6B indicate that the 3' ends of both Pol IV transcripts and RDR2 transcripts overhang the paired strand, fitting the predictions of the model in Figure 6A.

Because Pol IV transcripts within Pol IV-RDR2 dsRNAs are trimmed 1-2 nt by S1 nuclease at their 3' ends, this suggests that RDR2 initiates 1 or 2 nt internal to the ends of Pol IV transcripts. As a test of this hypothesis, we used a 5' end-labeled synthetic RNA as a template for recombinant RDR2 (Mishra et al., 2021) and subjected resulting dsRNA products to S1 nuclease digestion (Figure 6C). S1 trimmed the 5'-labeled template strand of the RNA duplexes by 1-2 nt (lanes 1 and 2). As controls, we synthesized RNA strands with perfect complementarity to the template strand (lanes 3 and 4) or were shorter by 1 (lanes 5 and 6) or 2 nt (lanes 7 and 8) at their 5' ends, annealed these RNAs to the 5' end-labeled template RNA strand, and subjected resulting dsRNAs to S1 nuclease digestion. S1 digestion patterns for synthetic dsRNAs with 1 or 2 nt overhangs most closely resembled the digestion patterns observed for RDR2 transcription products (compare lanes 2, 6 and 8). We conclude that RDR2 initiates transcription 1 or 2 nt

internal to the 3' ends of the Pol IV transcripts it uses as templates, consistent with the results of Figure 6B and scenarios 2 and 3 of Figure 6A.

Labeling Pol IV and RDR2 transcripts in different ways and observing how siRNAs were derived from the labeled precursor strands revealed that 24 and 23 nt siRNAs come from opposite ends of Pol IV and RDR2-transcribed RNA strands (Figure 6D). By initiating Pol IV-RDR2 transcription with an RNA primer labeled with ^{32}P on its 5' end, only the Pol IV strands of resulting dsRNAs are labeled (as in Figure 6B). Upon dicing of these dsRNAs into siRNAs, only labeled 24 nt siRNA products are detected (Figure 6D, lane 2). Note that a labeled band of ~25 nt is also apparent in lanes 1 and 2, but this is a Pol IV- and DCL3-independent RNA that results from RDR2 transcription of the 16 nt RNA primer, generating an initial transcript that folds back on itself into a partial stem-loop structure, followed by further elongation upon transcription of the single-stranded portion of the stem.

Unlike the dicing results obtained using end-labeled Pol IV strands, in which only labeled 24 nt siRNAs were detected following dicing, body-labeling of Pol IV or RDR2 strands yields labeled 24 and 23 siRNAs upon dicing (Figure 6D, lanes 4 and 6).

In a third labeling strategy, we initiated Pol IV transcripts using a dephosphorylated primer and unlabeled nucleotide triphosphates to generate Pol IV-RDR2 dsRNAs. Resulting dsRNAs were then diced by DCL3 and dicing products were subjected to capping reactions using vaccinia virus capping enzyme and ^{32}P-GTP to label siRNAs that retain the triphosphorylated 5' end of the RDR2 strand. In this experiment, only 24 nt siRNAs were capped with ^{32}P-GTP (Figure 6D, lane 10), suggesting that only 24 nt siRNAs come from the 5' ends of RDR2 transcripts.

Collectively, the experiments of Figure 6D reveal that siRNAs derived from the 5' ends of Pol IV transcripts and the 5' ends of RDR2 transcripts are 24 nt, consistent with DCL3 measuring and cutting 24 nt from the 5' end of either strand. We thus deduce that the 23 nt siRNA dicing products, which are observed only when Pol IV or RDR2 transcripts are body-labeled (lanes 4 and 6), come from the 3' ends of Pol IV and RDR2 transcripts.

Discussion

In vivo, highly abundant DCL3-dependent 24 and 23 nt siRNAs map to genomic loci subjected to RNA-directed DNA methylation, forming a swarm of overlapping siRNAs that make relationships between siRNAs of opposite polarity, or alternative size, very difficult to discern. Likewise, determining which siRNA precursor strands are synthesized by Pol IV and which are synthesized by RDR2 is problematic *in vivo*, as the enzymes work as a complex and are co-dependent (Blevins *et al.*, 2015; Singh *et al.*, 2019). Our *in vitro* biochemical experiments circumvent these uncertainties. Several important insights came from recapitulating siRNA biogenesis by incubating purified Pol IV, RDR2 and DCL3 with single-stranded bacteriophage M13 as the source of template DNA (Singh *et al.*, 2019). These experiments showed definitively that Pol IV acts first, transcribing the single-stranded template DNA to generate RNA transcripts whose 5' to 3' polarity is opposite that of the DNA. RDR2 acts second, using the Pol IV transcripts as templates to generate complementary RNAs that are oriented in the same 5' to 3' polarity as the DNA template strand, and thus could not have been directly transcribed from the DNA. The ability to unambiguously discriminate the Pol IV transcripts from the RDR2 transcripts, based on their polarity relative to the template DNA, also allowed strand-specificities of DCL3-diced siRNAs to be assigned. These studies showed that 24 and 23 nt siRNAs are generated from both the Pol IV and the RDR2-transcribed strands of siRNA precursors, with 24 nt siRNAs outnumbering 23 nt siRNAs by several fold (Singh *et al.*, 2019). Moreover, these studies showed that an untemplated nucleotide at the 3' terminus is a characteristic of RDR2 transcripts, but not Pol IV transcripts. The untemplated 3'-terminal nucleotide persists in siRNAs derived from RDR2 transcripts but, importantly, is selectively enriched among 23 nt siRNAs and not 24 nt siRNAs (Singh *et al.*, 2019). However, 23 nt siRNAs also come from the 3' ends of Pol IV transcripts (Figure 6D), helping explain why not all 23 nt siRNAs possess an untemplated nucleotide (Singh *et al.*, 2019; Wang et al., 2016).

The occurrence of an untemplated nucleotide at the end of 23 nt siRNAs derived from RDR2 transcripts led to the model in Figure 1B. In this model, diced 23 nt siRNAs derived from the 3' ends of RDR2 transcripts are paired with 24 nt siRNAs derived from the 5' ends of Pol IV transcripts. However, the model did not account for how 24 nt siRNAs can come from the RDR2 strand, explain why RDR2-strand 24 nt siRNAs outnumber 23 nt siRNAs, or account for 23 nt siRNAs derived from the Pol IV strand (Singh *et al.*, 2019). Our current study provides answers

to these questions. A key finding is that RDR2 does not initiate second strand RNA synthesis precisely at the 3' end of a Pol IV transcript, but 1-2 nt internal to the transcript. As a result, a 3' overhang of 1-2 nt is generated upon RDR2 initiation. A second key finding is that the 3'overhangs, attributable to RDR2's mode of initiation or its terminal transferase activity, generate preferred DCL3 substrates. Pol IV-RDR2 dsRNAs are typically shorter than 40 bp, thus they can be diced only once (Blevins *et al.*, 2015; Zhai *et al.*, 2015), either from the left side or right side. Our experiments reveal that this left/right choice is influenced by the 5' terminal nucleotide at the recessed end of an overhang, with adenosines or uridines favored over guanosines or cytosines. Importantly, Pol IV transcription tends to begin with a purine, with adenosine used somewhat more frequently than guanosine (Singh *et al.*, 2019). Collectively, our experiments suggest that if Pol IV initiates with an adenosine, left-side dicing is favored, with DCL3 generating a diced duplex consisting of a 24 nt siRNA from the 5' end of the Pol IV strand paired with a 23 nt siRNA from the 3' end of the RDR2 strand (Figure 7, dicing scenario 1). By contrast, if Pol IV transcription begins with a G, we propose that this encourages right-side dicing, especially if the RDR2 strand has a 5' A or U that is optimal for DCL3 engagement. Indeed, RNA-seq data have shown that RDR2 transcripts initiate most frequently with A or U (Singh *et al.*, 2019). Moreover, consensus sequences of *in vivo* precursor 5' and 3' ends best matched consensus sequences for siRNA 5' and 3' ends by invoking left-side dicing for precursors that initiated with A and right-side dicing for precursors that initiated with G (Blevins *et al.*, 2015). Our current study shows that it is this right-side dicing that accounts for 24 nt siRNAs derived from the RDR2 strand and 23 nt siRNAs derived from the Pol IV strand. There are two ways to generate 24 nt siRNAs from each strand and only one way to generate 23 nt siRNAs from each strand (Figures 6A and 7), which fits with the fact that 24 nt siRNAs are more abundant than 23 nt siRNAs, both *in vivo* and *in vitro* (Blevins *et al.*, 2015; Singh *et al.*, 2019).

Our study also provides new insight into the minimum length of Pol IV or RDR2 transcripts that can serve as siRNA precursors or siRNAs. The experiments of Figure 2 indicate that Pol IV transcripts that are 24 nt or longer are sufficient to give rise to DCL3-dependent siRNAs. Moreover, if Pol IV were to generate a 24 nt transcript and RDR2 were to initiate 2 nt internal to this transcript and add an extra untemplated nucleotide to the 3' end of its transcript, the result would be a 24/23 nt dsRNA duplex. This duplex would not need to be diced by DCL3 because it is already indistinguishable from a dicing product (see Figure 2C). Importantly, in

366 *dcl2 dcl3 dcl4* triple mutants, we detected Pol IV-dependent 24 nt RNAs at ~7% of the level
367 found in wild-type plants (Blevins *et al.*, 2015). This may account for low levels of RNA-
368 directed DNA methylation that persist in dicer mutants, suggesting an additional, or alternative,
369 explanation to proposed dicer-independent pathways that might be distinct from the canonical
370 RNA-directed DNA methylation pathway (Yang *et al.*, 2016; Ye *et al.*, 2016).
371 Another prior finding in need of reconsideration is the observation that 24 nt siRNAs
372 associated with AGO4 tend to begin with a 5' adenosine (Mi *et al.*, 2008), a finding that has been
373 interpreted as evidence that AGO4 actively selects siRNAs that begin with an adenosine. We
374 have shown that Pol IV and RDR2 transcripts most frequently begin with adenosine (Singh *et*
375 *al.*, 2019) and our current study shows that DCL3 preferentially dices substrates with A at their
376 5' ends. Thus Pol IV, RDR2 and DCL3 activities can collectively account for much of the 5' A-
377 bias among siRNAs that become loaded into AGO4, independent of AGO4-mediated selection.
378 Our results illustrate how siRNAs of different length can be produced by a Dicer
379 endonuclease that measures a fixed length of RNA, an apparent paradox. This fixed length
380 presumably corresponds to the distance from a phosphorylated or triphosphorylated 5' terminal
381 nucleotide, bound by the PAZ domain, as in other Dicers (Park et al., 2011; Sinha *et al.*, 2018;
382 Tian et al., 2014) to the RNase III domain B cleavage site of DCL3, a length equivalent to 24 nt.
383 The siRNAs of alternative size (23 nt) come from the opposite strand of RNA. The 5' end of the
384 non-measured strand is generated by the RNase III domain A cleavage reaction, but the 3' end of
385 this strand is apparently not anchored at a set distance, unlike human dicer (Park *et al.*, 2011),
386 and can overhang the 5' end of the measured strand by 1 nt, to yield a 23 nt siRNA, or 2 nt to
387 yield a 24 nt siRNA (see Figures 6A and 7).
388 Our study adds to our knowledge of how individual reactions within the RNA-directed
389 DNA methylation pathway specify what will happen in the next step. Pol IV and RDR2
390 physically interact (Mishra *et al.*, 2021) and their activities are tightly coupled such that Pol IV
391 transcripts are channeled directly to RDR2 (Singh *et al.*, 2019) rather than released. Lack of Pol
392 IV-interaction explains why the other five RNA-dependent RNA polymerases in *A. thaliana* are
393 not redundant with RDR2. Our current study now shows that idiosyncrasies of Pol IV and RDR2
394 transcription, including the choice of nucleotide used to initiate transcription, the alternative start
395 site positions of RDR2 internal to Pol IV transcripts, and the non-templated addition of a
396 nucleotide at the 3' end of RDR2 transcripts, collectively inform DCL3 how to dice the dsRNAs

at the next step of the pathway. This results in production of siRNAs that can be 23 or 24 nt, derived from either strand. Experimental evidence indicates that the specification of 23 and 24 nt siRNAs has functional significance, by specifying that the 24 RNA of a 23/24 nt RNA duplex become the siRNA stably associated with AGO4 (Wang and Pikaard, manuscript in preparation). Thus, by generating 24 and 23 nt siRNAs from either strand and either end of Pol IV-RDR2 dsRNAs, DCL3 can diversify the set of siRNAs that can be derived from short dsRNA precursors, enabling siRNA basepairing with Pol V transcripts transcribed from either strand of target loci DNA to maximize DNA methylation.

Acknowledgments

We thank the Drosophila Genome Resource Center at Indiana University for use of their insect cell culture facilities. This research was supported by NIH grant GM077590 and funds to CSP as an Investigator of the Howard Hughes Medical Institute. AL and JS were supported, in part, by Carlos O. Miller graduate fellowship funds of Indiana University.

Author Contributions

AL expressed and purified wild-type and mutant DCL3 proteins used in the study and performed all experiments of Figures 1-5. JS generated the data of Figures 6B and 6D. AF generated the data of Figure 6C. VM pioneered the expression of functional DCL3 and RDR2 to initiate the study. FW conducted analyses of RNA-seq data that contributed to the model of Figure 6A. AL and CP wrote the manuscript.

Declaration of Interests

The authors declare no competing interests.

Materials and Methods

Reagents and resources used in the study

A list of reagents or resources used, or generated, in the study, including supplier names and catalog numbers, is provided in Supplementary Table 3.

Overexpression and purification of recombinant DCL3

Recombinant FLAG epitope tagged DCL3 was expressed and purified as previously described (Singh *et al.*, 2019). Briefly, High Five™ insect cells (Thermo Fisher) were used to produce DCL3 using baculovirus mediated protein expression (MOI = 1.5). The baculovirus infected High Five cells were collected, pelleted at 500 x g for 5 min, flash-frozen in liquid nitrogen and stored at -80ºC. To purify DCL3, High Five cell pellets (~5 mL) were thawed on ice for 10-15 min and lysed using 45 mL hypertonic lysis buffer (50 mM HEPES-KOH (7.5), 400 mM NaCl, 5 mM $MgSO_4$, 10% glycerol, 2 mM DTT, 1 mM PMSF, 1% protease inhibitor cocktail, 0.01% IPEGAL® CA-630 (Sigma)). The lysate was centrifuged at 50,000 x g for 30 min at 4ºC. The supernatant was incubated with 0.5 mL anti-FLAG® M2 resin (Sigma) for 2 hrs at 4ºC. Beads were collected by centrifugation for 3 min at 300 x g at 4ºC and washed 3x as follows: 1x with 50 mL lysis buffer, 1x with 50 mL lysis buffer + 5 mM ATP·Mg^{2+} (Sigma), 1 x with 50 mL low salt wash buffer (50 mM HEPES-KOH (7.5), 150 mM NaCl, 5 mM $MgSO_4$, 10% glycerol, 1 mM DTT, 0.01% IPEGAL® CA-630). DCL3-bound FLAG resin was transferred to a small gravity-flow column, washed with 10 mL low salt buffer, and eluted 5x with 1 volume elution buffer (0.5 mg/mL 3x FLAG peptide, 50 mM HEPES-KOH (7.5), 150 mM NaCl, 5 mM $MgSO_4$, 10% glycerol, 1 mM DTT, 0.01% IPEGAL® CA-630). Eluted fractions were pooled and concentrated using a Centricon® filter (EMD Millipore) with a 30 kDa cutoff size and analyzed by electrophoresis on a 4-20% SDS-PAGE gel and Coomassie Blue staining. Recombinant DCL3 was stored at -20°C in storage buffer (50 mM HEPES-KOH (7.5), 150 mM NaCl, 5 mM $MgSO_4$, 45% glycerol, 1 mM DTT, 0.01% IPEGAL® CA-630).

To generate point mutations in the two RNase III domains, the wild-type DCL3 cDNA construct in pUC57 were mutated using site-directed, ligase independent mutagenesis. Resulting constructs were confirmed by sequencing. DCL3 sequences were then sub-cloned into the pFastBac™ HT B vector (Thermo Fisher) and bacmids and baculovirus were produced as

previously described (Singh *et al.*, 2019). Overexpression and purification of active-site mutants was performed as for the wild-type version of the protein.

Synthetic nucleic acids used in dicing assays

RNA oligonucleotides used in this study were purchased from Integrated DNA Technologies, Inc., with the exception of the 5' triphosphorylated oligo used in Figure 4C, which was purchased from BioSynthesis, Inc. Oligonucleotides used for dicing assays are listed in Supplementary Table 1.

RNA oligonucleotides were gel-purified using 15% denaturing polyacrylamide gel electrophoresis. As necessary, RNAs were monophosphorylated on their 5' ends using T4 polynucleotide kinase (NEB) and either 3 mM unlabeled ATP (Sigma) or 25 µCi of [γ32P] ATP, 6000 Ci/mmol (Perkin Elmer). Following PNK treatment, reactions were passed through Performa® spin columns (EdgeBio) at 1000 x g for 3 min. For non-radioactive dicing reactions, equimolar amounts of RNA oligos were mixed in annealing buffer (30 mM HEPES-KOH (7.6), 100 mM potassium acetate), whereas for radioactive dicing reactions a 10% excess of unlabeled oligos were mixed with ^{32}P-labeled oligos in annealing buffer. RNAs were incubated 5 min in an 85ºC water bath and annealed by allowing the water bath to cool to room temperature.

DCL3 dicing assays

Double-stranded RNA substrates were diced in 40 µL reactions containing either 25 nM (^{32}P-labeled) or 50 nM (nonradioactive) dsRNA substrate, 25 nM DCL3, 50 mM HEPES-KOH (7.5), 150 mM NaCl, 5 mM $MgSO_4$, 10% glycerol, 1 mM DTT, 0.01% IPEGAL® CA-630 and 0.4 U/µL RiboLock RNase Inhibitor (Thermo Fisher) for 30-60 min at room temperature and stopped by incubation at 72ºC for 5 min. Reactions were then passed through Performa® spin columns (EdgeBio) by centrifuging at 1000 x g for 3 min and adjusted to 0.3 M sodium acetate (5.2). 15 µg GlycoBlue™(Thermo Fisher) was added and RNAs were precipitated with 3 volumes of isopropanol at -20°C overnight. Precipitated RNAs were pelleted by centrifugation at 16,000 x g for 30 min, washed with 1 mL 70% ethanol, and resuspended in 10 µL 2x RNA Loading Dye (NEB). Resuspended RNAs were incubated at 72°C for five min and resolved on 15% polyacrylamide 7 M urea gels. For radioactive assays, gels were transferred to filter paper, vacuum dried, and subjected to phosphorimaging using a Typhoon scanner (GE Healthcare). For

non-radioactive assays, gels were stained with SYBR™ Gold (Invitrogen) in 0.5x TBE for 30 min at room temperature.

For time-course assays reactions were carried out as described above except 5 nM DCL3 was used and in 80-110 µL reaction volumes, depending on the number of time points assayed. To collect and stop reactions at each time point, 25 µL of all reactions were transferred simultaneously using a multichannel pipette to tubes containing 2 µL 0.5 M EDTA (8.0).

Pol IV-RDR2 transcription assays

To detect single-stranded regions of dsRNAs synthesized by Pol IV and RDR2, in vitro transcription reactions were performed as previously described (Singh et al., 2019). Oligonucleotides used for *in vitro* transcription reactions are listed in Supplementary Table 2. Resulting Pol IV-RDR2 dsRNAs were then subjected to the indicated amounts of S1 nuclease (Thermo Fisher) digestion for 10 min at 37°C using the manufacturer supplied S1 nuclease digestion buffer. Following this, RNAs were precipitated with 3 volumes of isopropanol, 1/10th volume of 3M sodium acetate (5.2), 20 µg of GlycoBlue™ (Thermo Fisher) and overnight incubation at -20°C. Precipitated RNAs were pelleted by centrifugation 16,000 x g for 30 min, washed with 1 mL 70% ethanol, and resuspended in 2x RNA Loading Dye (NEB). Resuspended RNAs were incubated at 72°C for 5 min and loaded onto a 15% polyacrylamide 7 M urea gel. Following electrophoresis, gels were transferred to filter paper, vacuum dried, and subjected to autoradiography using BioMax® XAR film (Kodak).

Dicing and capping of siRNAs generated from in vitro Pol IV-RDR2-DCL3 reactions were performed as previously described (Singh et al., 2019).

RDR2 transcription assays

Recombinant RDR2 was expressed and purified as previously described (Blevins et al., 2015). For RDR2 transcription reactions, recombinant RDR2 (280 nM) was mixed with 5' ^{32}P-labeled template strand RNA (50 nM) in a 30 µL reaction containing 25 mM HEPES-KOH (pH 7.9), 20 mM ammonium acetate, 50 mM NaCl, 2 mM $MgCl_2$, 0.4 U/ µL RNase Inhibitor (NEB), 0.1 mM EDTA, 0.01% Triton X-100, 3% PEG8000 and 0.1 mM each of GTP, CTP, UTP and ATP. Reactions were incubated at room temperature for 2 hrs. Then, the reaction products were split into 10 µL aliquots and S1 nuclease 10x reaction buffer (Promega) was added to 1x

concentration. Following this, S1 nuclease (Promega) or an equivalent amount of 1x S1 nuclease reaction buffer was added. After incubation at 37°C for 15 min, reactions were stopped by addition of 50 µL of Proteinase K solution (100 mM Tris-HCl (7.9), 250 mM NaCl, 1 mM $MgCl_2$, 1% SDS, 0.4 mg/mL Proteinase K RNA grade (Invitrogen), 0.3 mg/mL GlycoBlue™ (Thermo Fisher)) and incubated for an additional 30 min at 37°C. RNAs were then precipitated by adding 180 µL 100% ethanol and incubating overnight at -20°C. Precipitated RNAs were pelleted by centrifugation at 16,000 x g for 20 min, washed with 300 µL 70% ethanol, and resuspended in 10 µL 2x TBE-Urea Sample Buffer (Invitrogen). Resuspended RNAs were incubated at 75°C for five min, snap-cooled on ice and resolved on 15% polyacrylamide 7 M urea gels. Gels were transferred to filter paper, vacuum dried, and subjected to phosphorimaging using a Typhoon™ scanner (GE Healthcare).

Quantification and statistical analysis

DCL3 assays were quantified using Image Lab version 6.0 software (Bio-Rad Laboratories). Substrate and diced RNA bands were boxed and diced band signal calculated as the % of total signal. In Figure 4, means for triplicate reactions are plotted, with error bars showing the standard error of the mean.

Data Availability

Raw gel images and excel files for quantitative analyses shown in the figures in the paper are provided as source files in the Supplementary Information.

Additional Files

Supplementary Table 1
Supplementary Table 2
Supplementary Table 3
Figure 1-figure supplement 1
Figure 3-figure supplement 1
Figure 1 source data-zipped folder
Figure 2 source data-zipped folder
Figure 3A and 3B source data-zipped folder
Figure 4A source data-zipped folder
Figure 4B source data -zipped folder
Figure 4C source data -zipped folder
Figure 5 source data-zipped folder
Figure 6 source data -zipped folder

References

Blevins, T., Podicheti, R., Mishra, V., Marasco, M., Tang, H., and Pikaard, C.S. (2015). Identification of Pol IV and RDR2-dependent precursors of 24 nt siRNAs guiding de novo DNA methylation in Arabidopsis. Elife *4*, e09591. 10.7554/eLife.09591.

Cao, X., and Jacobsen, S.E. (2002). Role of the Arabidopsis DRM Methyltransferases in De Novo DNA Methylation and Gene Silencing. Curr Biol *12*, 1138-1144.

El-Shami, M., Pontier, D., Lahmy, S., Braun, L., Picart, C., Vega, D., Hakimi, M.A., Jacobsen, S.E., Cooke, R., and Lagrange, T. (2007). Reiterated WG/GW motifs form functionally and evolutionarily conserved ARGONAUTE-binding platforms in RNAi-related components. Genes Dev *21*, 2539-2544.

Haag, J.R., Ream, T.S., Marasco, M., Nicora, C.D., Norbeck, A.D., Pasa-Tolic, L., and Pikaard, C.S. (2012). In vitro transcription activities of Pol IV, Pol V, and RDR2 reveal coupling of Pol IV and RDR2 for dsRNA synthesis in plant RNA silencing. Mol Cell *48*, 811-818. 10.1016/j.molcel.2012.09.027.

Havecker, E.R., Wallbridge, L.M., Hardcastle, T.J., Bush, M.S., Kelly, K.A., Dunn, R.M., Schwach, F., Doonan, J.H., and Baulcombe, D.C. (2010). The Arabidopsis RNA-directed DNA methylation argonautes functionally diverge based on their expression and interaction with target loci. Plant Cell *22*, 321-334. tpc.109.072199 [pii] 10.1105/tpc.109.072199.

Henderson, I.R., Zhang, X., Lu, C., Johnson, L., Meyers, B.C., Green, P.J., and Jacobsen, S.E. (2006). Dissecting Arabidopsis thaliana DICER function in small RNA processing, gene silencing and DNA methylation patterning. Nat Genet *38*, 721-725. ng1804 [pii] 10.1038/ng1804.

Ipsaro, J.J., and Joshua-Tor, L. (2015). From guide to target: molecular insights into eukaryotic RNA-interference machinery. Nat Struct Mol Biol *22*, 20-28. 10.1038/nsmb.2931.

Kasschau, K.D., Fahlgren, N., Chapman, E.J., Sullivan, C.M., Cumbie, J.S., Givan, S.A., and Carrington, J.C. (2007). Genome-wide profiling and analysis of Arabidopsis siRNAs. PLoS Biol *5*, e57.

587 Lahmy, S., Pontier, D., Bies-Etheve, N., Laudie, M., Feng, S., Jobet, E., Hale, C.J., Cooke, R.,
588 Hakimi, M.A., Angelov, D., et al. (2016). Evidence for ARGONAUTE4-DNA interactions in RNA-
589 directed DNA methylation in plants. Genes Dev *30*, 2565-2570. 10.1101/gad.289553.116.
590 Law, J.A., Vashisht, A.A., Wohlschlegel, J.A., and Jacobsen, S.E. (2011). SHH1, a homeodomain
591 protein required for DNA methylation, as well as RDR2, RDM4, and chromatin remodeling
592 factors, associate with RNA polymerase IV. PLoS Genet *7*, e1002195.
593 10.1371/journal.pgen.1002195.
594 Li, S., Vandivier, L.E., Tu, B., Gao, L., Won, S.Y., Li, S., Zheng, B., Gregory, B.D., and Chen, X.
595 (2015). Detection of Pol IV/RDR2-dependent transcripts at the genomic scale in Arabidopsis
596 reveals features and regulation of siRNA biogenesis. Genome Res *25*, 235-245.
597 10.1101/gr.182238.114.
598 Martienssen, R., and Moazed, D. (2015). RNAi and heterochromatin assembly. Cold Spring Harb
599 Perspect Biol *7*, doi: 10.1101/cshperspect.a019323. 10.1101/cshperspect.a019323.
600 Matzke, M.A., and Mosher, R.A. (2014). RNA-directed DNA methylation: an epigenetic pathway
601 of increasing complexity. Nat Rev Genet *15*, 394-408. 10.1038/nrg3683.
602 Mi, S., Cai, T., Hu, Y., Chen, Y., Hodges, E., Ni, F., Wu, L., Li, S., Zhou, H., Long, C., et al. (2008).
603 Sorting of small RNAs into Arabidopsis argonaute complexes is directed by the 5' terminal
604 nucleotide. Cell *133*, 116-127. S0092-8674(08)00285-7 [pii]
605 10.1016/j.cell.2008.02.034.
606 Mishra, V., Singh, J., Wang, F., Zhang, Y., Fukudome, A., Trinidad, J.C., Takagi, Y., and Pikaard,
607 C.S. (2021). Assembly of a dsRNA synthesizing complex: RNA-DEPENDENT RNA POLYMERASE 2
608 contacts the largest subunit of NUCLEAR RNA POLYMERASE IV. Proc Natl Acad Sci U S A *118*.
609 10.1073/pnas.2019276118.
610 Mosher, R.A., Schwach, F., Studholme, D., and Baulcombe, D.C. (2008). PolIVb influences RNA-
611 directed DNA methylation independently of its role in siRNA biogenesis. Proc Natl Acad Sci U S
612 A *105*, 3145-3150.
613 Nagano, H., Fukudome, A., Hiraguri, A., Moriyama, H., and Fukuhara, T. (2014). Distinct
614 substrate specificities of Arabidopsis DCL3 and DCL4. Nucleic Acids Res *42*, 1845-1856.
615 10.1093/nar/gkt1077.

616 Park, J.E., Heo, I., Tian, Y., Simanshu, D.K., Chang, H., Jee, D., Patel, D.J., and Kim, V.N. (2011).
617 Dicer recognizes the 5' end of RNA for efficient and accurate processing. Nature *475*, 201-205.
618 10.1038/nature10198.
619 Ream, T.S., Haag, J.R., Wierzbicki, A.T., Nicora, C.D., Norbeck, A.D., Zhu, J.K., Hagen, G.,
620 Guilfoyle, T.J., Pasa-Tolic, L., and Pikaard, C.S. (2009). Subunit compositions of the RNA-silencing
621 enzymes Pol IV and Pol V reveal their origins as specialized forms of RNA polymerase II. Mol Cell
622 *33*, 192-203. 10.1016/j.molcel.2008.12.015.
623 Shabalina, S.A., and Koonin, E.V. (2008). Origins and evolution of eukaryotic RNA interference.
624 Trends in ecology & evolution *23*, 578-587. 10.1016/j.tree.2008.06.005.
625 Singh, J., Mishra, V., Wang, F., Huang, H.Y., and Pikaard, C.S. (2019). Reaction Mechanisms of
626 Pol IV, RDR2, and DCL3 Drive RNA Channeling in the siRNA-Directed DNA Methylation Pathway.
627 Mol Cell *75*, 576-589 e575. 10.1016/j.molcel.2019.07.008.
628 Singh, J., and Pikaard, C.S. (2019). Reconstitution of siRNA Biogenesis In Vitro: Novel Reaction
629 Mechanisms and RNA Channeling in the RNA-Directed DNA Methylation Pathway. Cold Spring
630 Harb Symp Quant Biol *84*, 195-201. 10.1101/sqb.2019.84.039842.
631 Sinha, N.K., Iwasa, J., Shen, P.S., and Bass, B.L. (2018). Dicer uses distinct modules for
632 recognizing dsRNA termini. Science *359*, 329-334. 10.1126/science.aaq0921.
633 Takeshita, D., Zenno, S., Lee, W.C., Nagata, K., Saigo, K., and Tanokura, M. (2007). Homodimeric
634 structure and double-stranded RNA cleavage activity of the C-terminal RNase III domain of
635 human dicer. J Mol Biol *374*, 106-120. 10.1016/j.jmb.2007.08.069.
636 Tian, Y., Simanshu, D.K., Ma, J.B., Park, J.E., Heo, I., Kim, V.N., and Patel, D.J. (2014). A
637 phosphate-binding pocket within the platform-PAZ-connector helix cassette of human Dicer.
638 Mol Cell *53*, 606-616. 10.1016/j.molcel.2014.01.003.
639 Wang, F., Johnson, N.R., Coruh, C., and Axtell, M.J. (2016). Genome-wide analysis of single non-
640 templated nucleotides in plant endogenous siRNAs and miRNAs. Nucleic Acids Res *44*, 7395-
641 7405. 10.1093/nar/gkw457.
642 Wendte, J.M., and Pikaard, C.S. (2017). The RNAs of RNA-directed DNA methylation. Biochim
643 Biophys Acta *1860*, 140-148. 10.1016/j.bbagrm.2016.08.004.

644 Wierzbicki, A.T., Haag, J.R., and Pikaard, C.S. (2008). Noncoding transcription by RNA
645 polymerase Pol IVb/Pol V mediates transcriptional silencing of overlapping and adjacent genes.
646 Cell *135*, 635-648. S0092-8674(08)01192-6 [pii]
647 10.1016/j.cell.2008.09.035.
648 Wierzbicki, A.T., Ream, T.S., Haag, J.R., and Pikaard, C.S. (2009). RNA polymerase V transcription
649 guides ARGONAUTE4 to chromatin. Nature genetics *41*, 630-634. 10.1038/ng.365.
650 Xie, Z., Johansen, L.K., Gustafson, A.M., Kasschau, K.D., Lellis, A.D., Zilberman, D., Jacobsen, S.E.,
651 and Carrington, J.C. (2004). Genetic and functional diversification of small RNA pathways in
652 plants. PLoS Biol *2*, doi: 10.1371/journal.pbio.0020104.
653 Yang, D.L., Zhang, G., Tang, K., Li, J., Yang, L., Huang, H., Zhang, H., and Zhu, J.K. (2016). Dicer-
654 independent RNA-directed DNA methylation in Arabidopsis. Cell Res *26*, 66-82.
655 10.1038/cr.2015.145.
656 Ye, R., Chen, Z., Lian, B., Rowley, M.J., Xia, N., Chai, J., Li, Y., He, X.J., Wierzbicki, A.T., and Qi, Y.
657 (2016). A Dicer-Independent Route for Biogenesis of siRNAs that Direct DNA Methylation in
658 Arabidopsis. Mol Cell *61*, 222-235. 10.1016/j.molcel.2015.11.015.
659 Zhai, J., Bischof, S., Wang, H., Feng, S., Lee, T.F., Teng, C., Chen, X., Park, S.Y., Liu, L., Gallego-
660 Bartolome, J., et al. (2015). A One Precursor One siRNA Model for Pol IV-Dependent siRNA
661 Biogenesis. Cell *163*, 445-455. 10.1016/j.cell.2015.09.032.
662 Zhang, H., Kolb, F.A., Jaskiewicz, L., Westhof, E., and Filipowicz, W. (2004). Single processing
663 center models for human Dicer and bacterial RNase III. Cell *118*, 57-68.
664 10.1016/j.cell.2004.06.017.
665 Zhang, X., Henderson, I.R., Lu, C., Green, P.J., and Jacobsen, S.E. (2007). Role of RNA polymerase
666 IV in plant small RNA metabolism. Proc Natl Acad Sci U S A *104*, 4536-4541.
667 Zhong, X., Du, J., Hale, C.J., Gallego-Bartolome, J., Feng, S., Vashisht, A.A., Chory, J.,
668 Wohlschlegel, J.A., Patel, D.J., and Jacobsen, S.E. (2014). Molecular mechanism of action of
669 plant DRM de novo DNA methyltransferases. Cell *157*, 1050-1060. 10.1016/j.cell.2014.03.056.
670 Zilberman, D., Cao, X., and Jacobsen, S.E. (2003). ARGONAUTE4 control of locus-specific siRNA
671 accumulation and DNA and histone methylation. Science *299*, 716-719.
672

Figure titles and legends

Figure 1. DCL3 preferentially dices double-stranded RNAs with 3' overhangs

A. A simplified model of RNA-directed DNA methylation (RdDM) highlighting the roles of Pol IV, Pol V, RDR2, DCL3 and AGO4.

B. Model depicting the hypothesis that DCL3 dicing of dsRNA precursors can yield a 24 nt siRNA from the 5' end of the Pol IV transcript paired to a 23 nt siRNA from the RDR2 3' end. Pol IV transcripts tend to begin with A or G and RDR2 transcripts often have an untemplated nucleotide (N) at their 3' termini. Green shading depicts DCL3 and its interaction with the left side of the dsRNA precursor.

C. A test of the model shown in panel B. A 37 nt top strand was annealed to 37, 38 or 39 nt bottom strand to form dsRNA substrates with two blunt ends or a left-side 1 or 2 nt 3' overhang on the bottom strand (see Supplementary Table 1 for RNA strand equences). Resulting dsRNAs (50 nM) were then incubated with 25 nM of affinity purified recombinant DCL3 (see Figure 1-figure supplement 1-panel A). RNAs were then resolved by denaturing polyacrylamide gel electrophoresis (PAGE) and visualized using SYBR Gold staining. Lane 4 is a control that includes DCL3 but no RNA.

D. DCL3 prefers 3' overhangs. Dicing reactions were conducted as in panel C, but with either the top strand (37 nt) or bottom strand (38 or 39 nt) 5' end-labeled with ^{32}P and the final concentration of dsRNAs being 25 nM. In each case, a non-radioactive monophosphate is also present at the 5' end of the complementary strand. Following incubation with (lanes 3,4,7,8) or without (lanes 1, 2, 5, and 6) DCL3, RNAs were resolved by denaturing PAGE and visualized by phosphorimaging. A related experiment comparing time courses of DCL3 cleavage for substrates with 1nt or 2 nt overhangs is shown in Figure 1-figure supplement 1- panel B.

E. DCL3 cuts from both ends of precursors that have two blunt ends. Dicing reactions of 5' end-labeled dsRNAs were conducted as in panel E but with precursors that lack a 3' overhang at one end.

Figure 2. DCL3 measures 24 nt from the recessed 5' end of a dsRNA with a 3' overhang.

In the experiments shown in each panel of the figure, RNA strands ranging in size from 22-25 nt were annealed in various permutations to form dsRNA substrates that were then tested for DCL3 dicing. RNA substrates and dicing products were then resolved by denaturing polyacrylamide gel electrophoresis and visualized by SYBR Gold staining.

A. Precursors as short as 24 and 25 nt can give rise to siRNAs. In this experiment, RNAs of 24 and 25 nt were annealed and tested for dicing. The diagram summarizes DCL3's trimming of 2 nt from the 3' end of the 25 nt RNA strand to generate a 24/23 nt dsRNA.

B. A recessed 5' end allows a 23 nt RNA to guide dicing consistent with the 24 nt measurement rule. RNAs of 24 nt or 23 nt RNAs were annealed to form a 24/24 nt (top strand/bottom strand) dsRNA with two blunt ends or a 23/24 nt dsRNA with a left-side 3' overhang. The diagram summarizes DCL3's trimming of 2 nt from the 5' end of either strand of 24/24 nt dsRNAs but trimming of 1 nt from the 24 nt strand of the 23/24 nt dsRNA substrate.

C. Predicted dicing products are not diced further by DCL3. Double-stranded RNAs with strands of 23 or 24 nt were annealed to generate 3' overhangs of 1 or 2 nt at each end. The 24/23 nt dsRNA mimics the digestion product introduced in Figure 1B. The 24/24 nt dsRNA mimics a product that might result from sequential dicing events or internal initiation by RDR2.

D. Duplexes in which both strands are 23 nt or shorter are not precisely diced but are digested by DCL3 into 17-22 nt products. Test substrates were 23/23 and 22/22 nt duplexes with two blunt ends, or a 22/23 nt duplex with a 1 nt 3' overhang on the bottom strand.

Figure 3. Strand cutting specificities of DCL3's RNase III domains.

A. Relative positions of helicase, PAZ, RNase III, and dsRNA binding domains within the 1508 amino acid sequence of DCL3. Positions of catalytic glutamate residues of RNase III domain A (E1146) and RNase III domain B (E1329) are highlighted. These glutamates were mutated to glutamine to generate catalytically inactive versions of DCL3.

B. Identification of dsRNA strands cut by the RNase IIIA and RNase III B domains of DCL3. A 26/27 nt dsRNA substrate, possessing a 1 nt 3' overhang, was subjected to dicing using wild-type DCL3 or the E1146Q and/or E1329Q mutant versions of DCL3. Lanes 1-4 are DCL3-only controls and lane 5 is a RNA-only control. DCL3 with wild-type RNase III domains A and B (denoted as +, +) was tested in lanes 1 and 6. DCL3 mutants with both RNase III domains mutated (denoted as -, -) was tested in lanes 2 and 7. Mutants with only wild-type RNase III domain were tested in lanes 3,4,8 and 9).

C. Model for DCL3 substrate recognition, 24 nt strand measurement and dicing.

Figure 4. DCL3 substrate recognition is influenced by 5' terminal nucleotide and phosphorylation status.

A. Test of top strand 5' nucleotide preference on dicing efficiency. Top strands of 37 nt that differ by having either A, U, C or G at their 5' termini were 5' end-labeled with ^{32}P and annealed to complementary 38 nt bottom strand RNAs to generate 1 nt 3' overhangs on the left side, as drawn. Following incubation with DCL3 for 1, 5 or 10 minutes, reaction products were resolved by non-denaturing PAGE and visualized by autoradiography. The diagram highlights the position of the labeled 24 nt dicing product measured in the assay.

B. Test of bottom strand 3' terminal nucleotide on dicing efficiency. This experiment was conducted as in panel A except that bottom strands had either A, U, C or G at their 3' termini, which overhang the top strand (5' A) by 1 nt.

C. Test of top strand 5' end phosphorylation on dicing efficiency. Two 37 nt RNA strands with adenosines at their 5' termini were annealed to generate dsRNAs with 3' overhangs of 1 nt at either end, encouraging DCL3 to dice from either end. The top strand was end-labeled with a ^{32}P monophosphate group whereas the 5'-terminal adenosine of the bottom strand had either a hydroxyl group (OH), a monophosphate (P) or a triphosphate (PPP). Left-side versus right-side

751 dicing was then assessed by the ratio of labeled 24 nt or 16 nt dicing products following non-
752 denaturing PAGE and autoradiography.
753
754
755 **Figure 5. DCL3 dicing does not require ATP**
756 A 37 nt top strand end-labeled with ^{32}P was annealed to 37, 38 or 39 nt bottom strands to
757 generate dsRNAs with blunt ends on the right side and either a blunt end or 3' overhangs of 1 or
758 2 nt on the left side. Resulting dsRNAs were then subjected to DCL3 dicing in the absence (-) or
759 presence (+) of ATP or the non-hydrolysable ATP analog, ATP-γ-S. Production of labeled 24 nt
760 dicing products were then assessed by denaturing PAGE and autoradiography.
761

Figure 6. Overhangs at both ends of DCL3 substrates explain 24 and 23 nt siRNA biogenesis from both strands.

A. Hypotheses to account for 24 and 23 nt siRNAs derived from both the Pol IV and RDR2-transcribed strands of diced dsRNAs. Scenario 1 is the hypothesis of Figure 1B and Singh et al., 2019, accounting for 23 nt RDR2-strand siRNAs bearing an untemplated 3' terminal nucleotide paired with 24 nt siRNAs corresponding to the 5' end of Pol IV transcripts. Scenarios 2 and 3 show how RDR2 transcription initiating either 1 nt or 2 nt internal to the 3' end of Pol IV transcripts could generate 3' overhangs of 1 or 2 nt, respectively, promoting right-side dicing. In Scenario 2, a 23 nt siRNA can be generated from the Pol IV strand and a 24 nt siRNA can be produced from the RDR2 strand. In scenario 3, 24 nt siRNAs are generated from both strands.

B. 3' overhangs are present at both termini of Pol IV-RDR2 transcribed dsRNAs.

Pol IV-RDR2 transcription reactions were performed in either of two ways to selectively label either the Pol IV or RDR2 strand. To label Pol IV transcripts, a ^{32}P-end-labeled RNA primer was used to initiate Pol IV transcription of a DNA template lacking thymidines (lanes 1-4). The presence of non-template DNA annealed to the template induces Pol IV arrest and RDR2 initiation of the complementary strand which can be selectively body-labeled using alpha-^{32}P-ATP (lanes 5-8). Overhangs present in the dsRNA products generated by the coupled reactions of Pol IV and RDR2 are sensitive to digestion by S1 nuclease treatment (see diagram), generating the shorter labeled products observed for both Pol IV (lanes 2-4) and RDR2 (lanes 6-8) transcripts. Mock S1 nuclease treatment negative controls are shown in lanes 1 and 2. RNAs were resolved by denaturing PAGE and visualized by autoradiography.

C. RDR2 initiates transcription 1 or 2 nt internal to the 3' end of the template RNA strand.

A 37 nt RNA labeled with ^{32}P at its 5' end (50 nM) was used as template for second strand synthesis by recombinant RDR2 (280 nM)(lanes 1 and 2). Half of the transcription reaction was then subjected to S1 nuclease digestion (lane 2). In parallel, controls in which the end-labeled template was hybridized with strands whose complementarity begins at the very end of the template or 1 or 2 nt internal were also generated and subjected to S1 nuclease digestion (lanes 3-8). RNAs were resolved by denaturing PAGE and visualized by autoradiography.

D. 24 nt siRNAs are diced from the 5' ends of Pol IV and RDR2 transcripts and 23 nt siRNAs are diced from their 3' ends. In vitro transcription reactions using the template, non-template and primer diagrammed in panel B (see Supplementary Table 2 for their sequences) were conducted

in several ways in order to specifically end-label or body-label Pol IV or RDR2 transcripts. The reactions of lanes 1 and 2 were conducted with end-labeled primer in order to specifically label the 5' ends of Pol IV transcripts. The labeled band of ~25 nt in both lanes 1 and 2 is an RDR2-dependent, Pol IV- and DCL3-independent background RNA. In lanes 3-6, unlabeled primer was used to initiate dsRNA synthesis from the T-less DNA template, with Pol IV or RDR2 transcripts body-labeled with either ^{32}P-UTP or ^{32}P-ATP, respectively. In the reactions of lanes 7-10, an unlabeled primer with a 5' hydroxyl group was used to initiate Pol IV transcription from the T-less DNA template. In the reactions of lanes 7 and 8, RDR2-transcripts were body labeled using ^{32}P-ATP (as in lanes 5 and 6). For the reactions in lanes 9 and 10, no labeled nucleotide was incorporated during transcription, but transcripts (lane 9) or dicing reactions (lane 10) were subsequently incubated with capping enzyme and alpha-^{32}P-GTP to label the 5' end of RDR2 transcripts by capping.

Figure 7. Summary model for a DCL3 dicing code that diversifies the siRNA pool guiding RNA-directed DNA methylation.

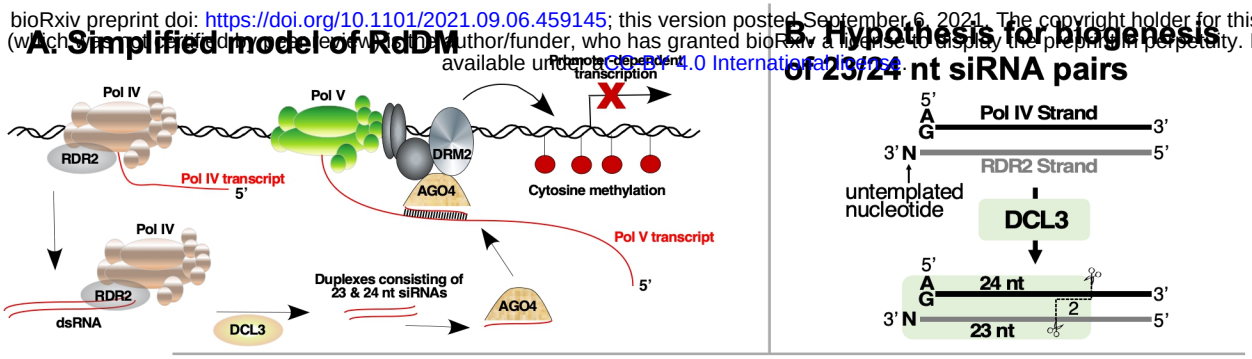

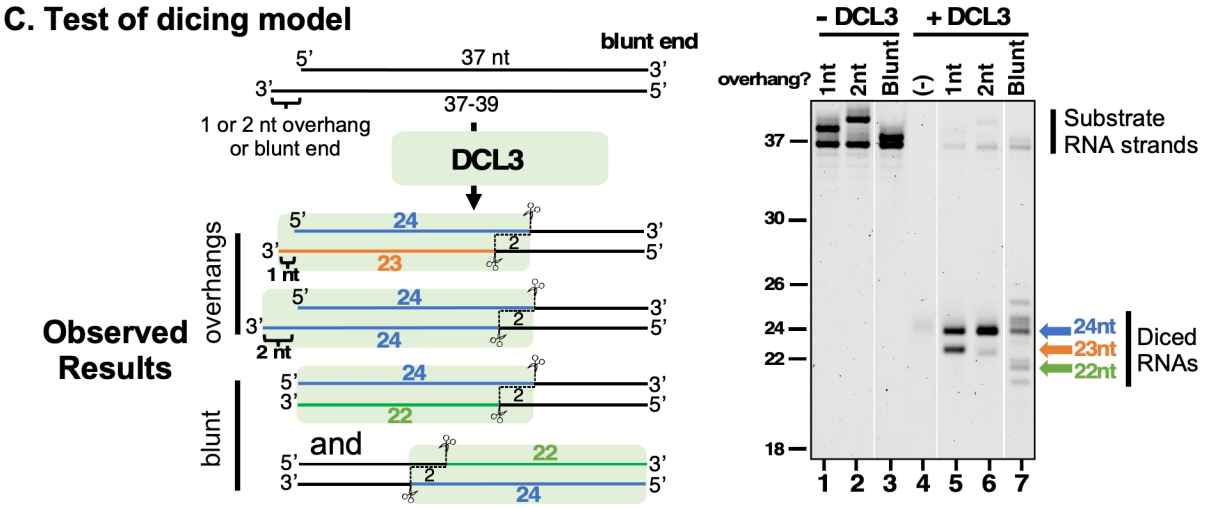

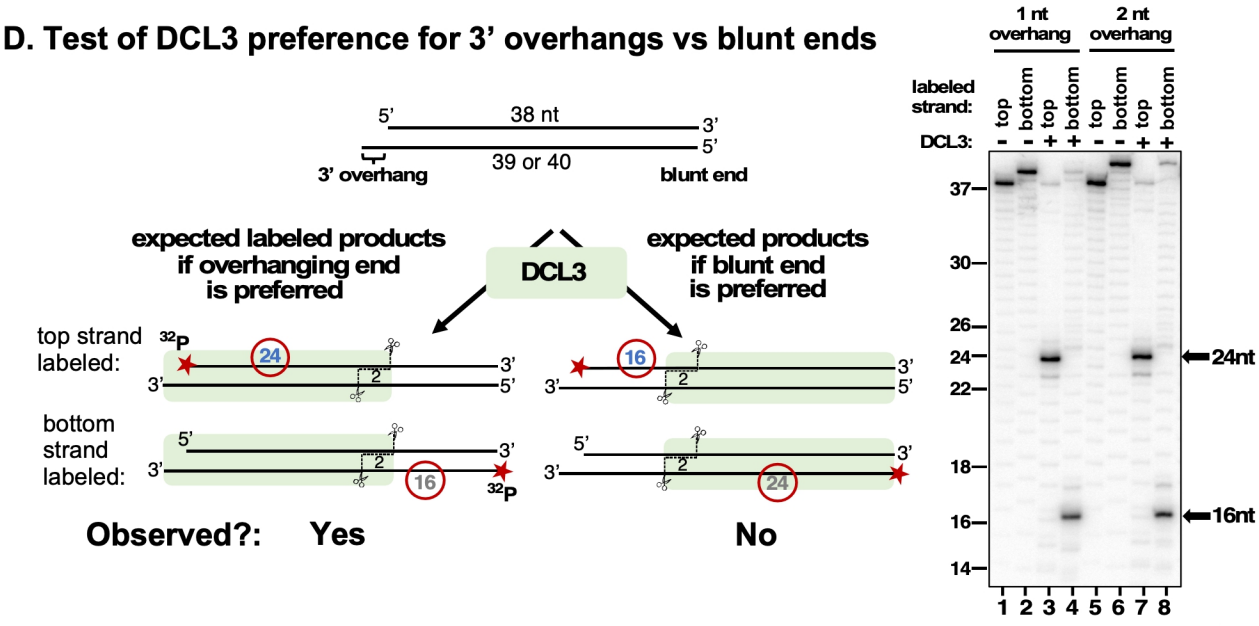

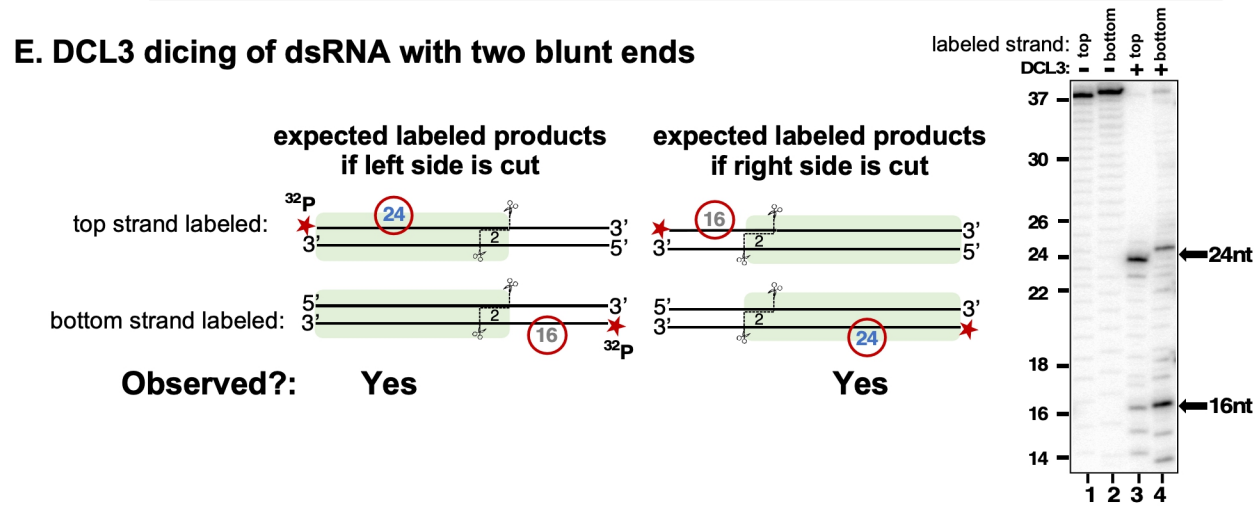

Loffer et al., Figure 1

A. Dicing of 24/25 duplex

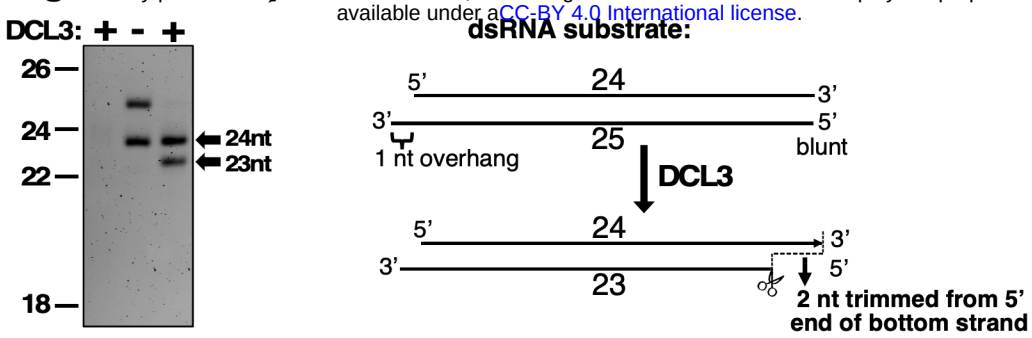

B. Dicing of 24/24 and 23/24 duplexes

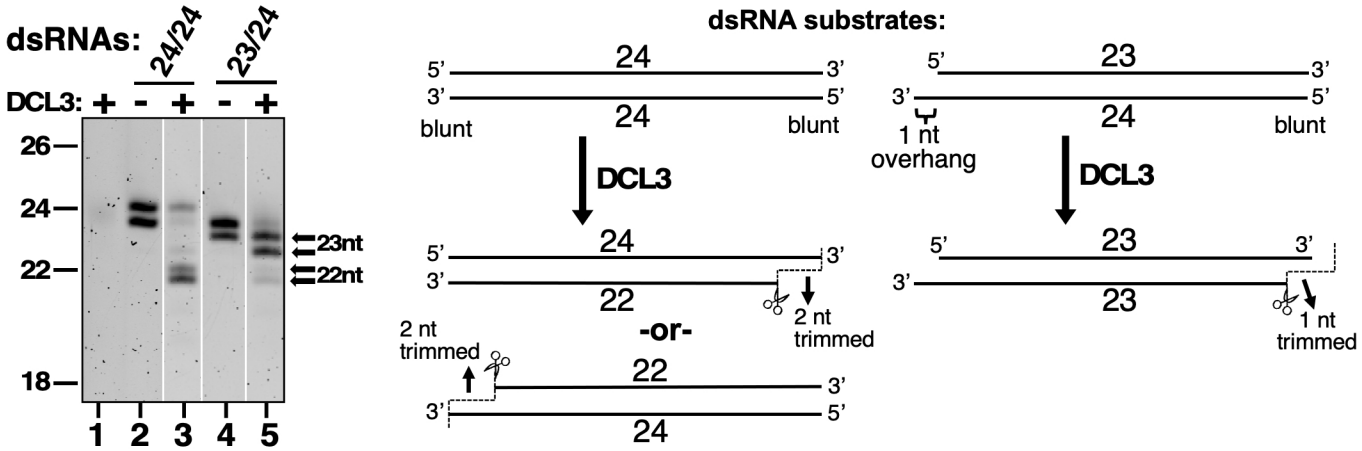

C. Test of predicted dicing products as dicing substrates

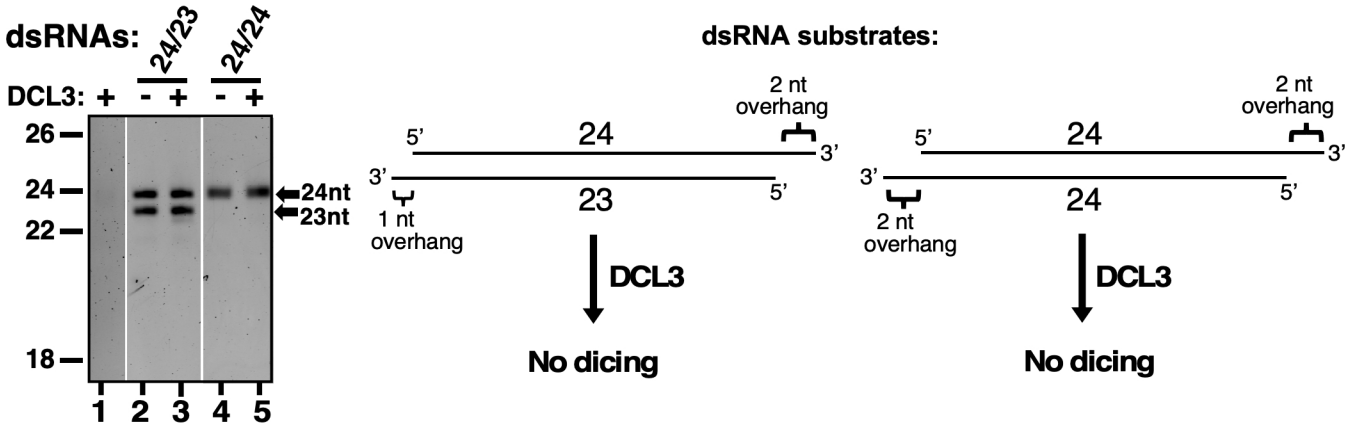

D. Imprecise digestion of dsRNAs with strands of 23 nt or shorter

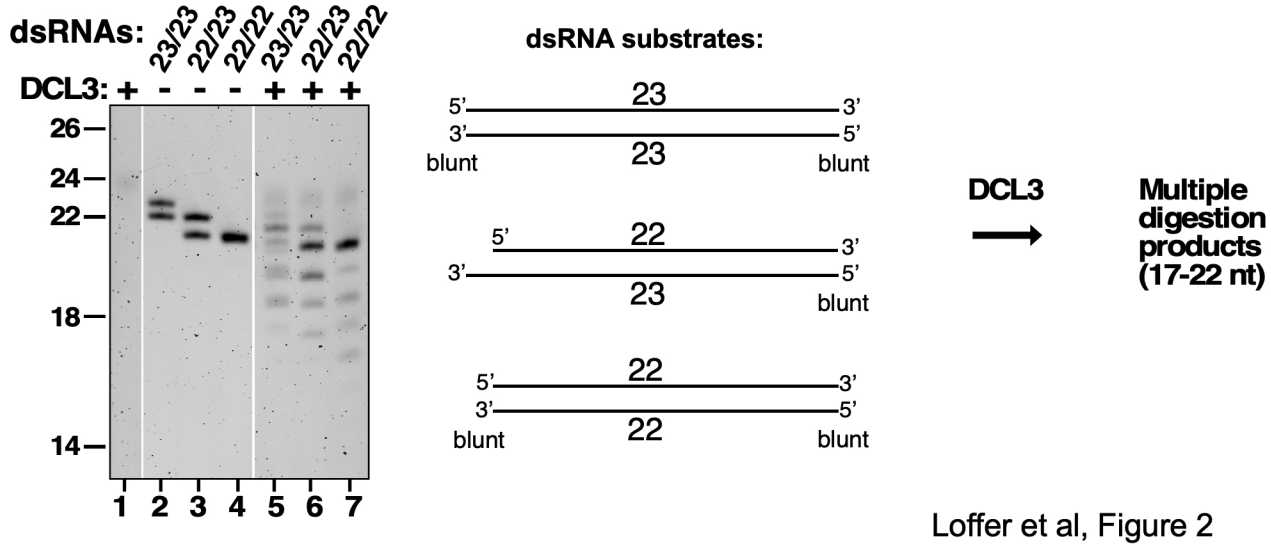

Loffer et al, Figure 2

A. DCL3 domain arrangement

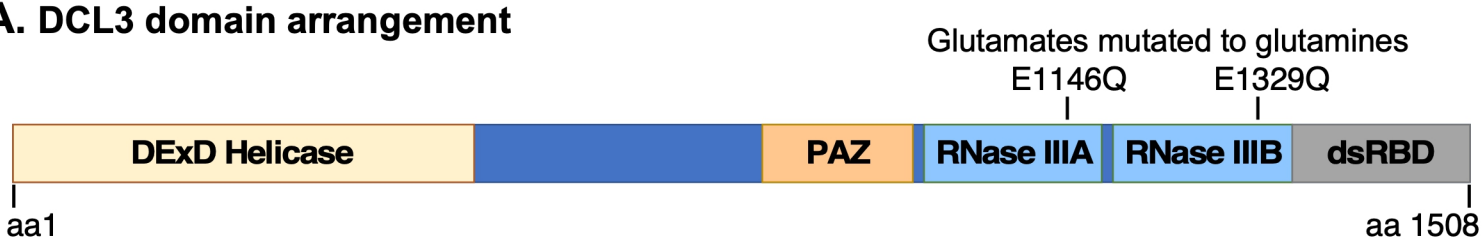

B. Identification of RNA strands cut by RNase IIIA and RNase III B domains

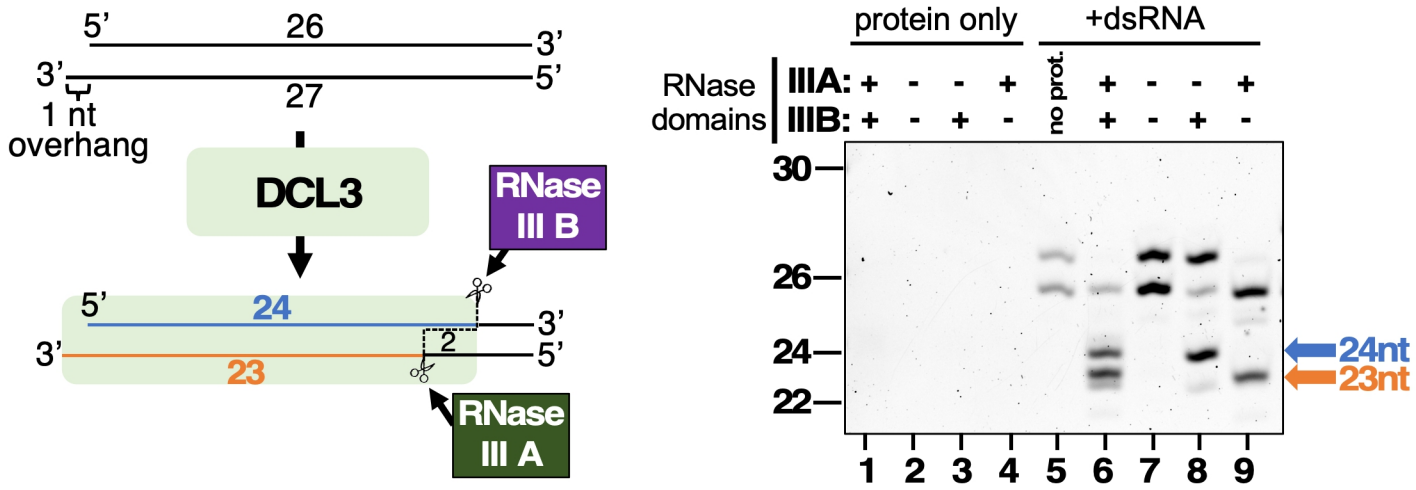

C. Summary model for DCL3 substrate recognition and dicing

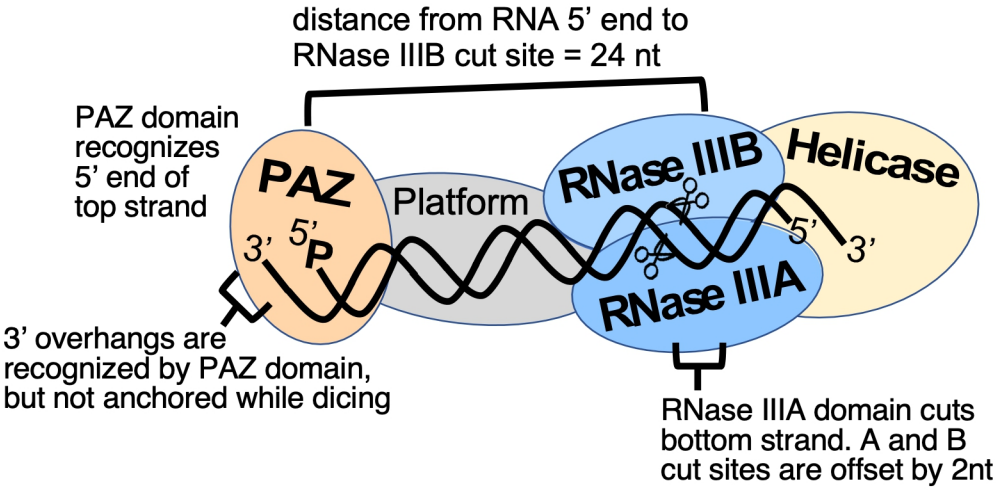

Loffer et al, Figure 3

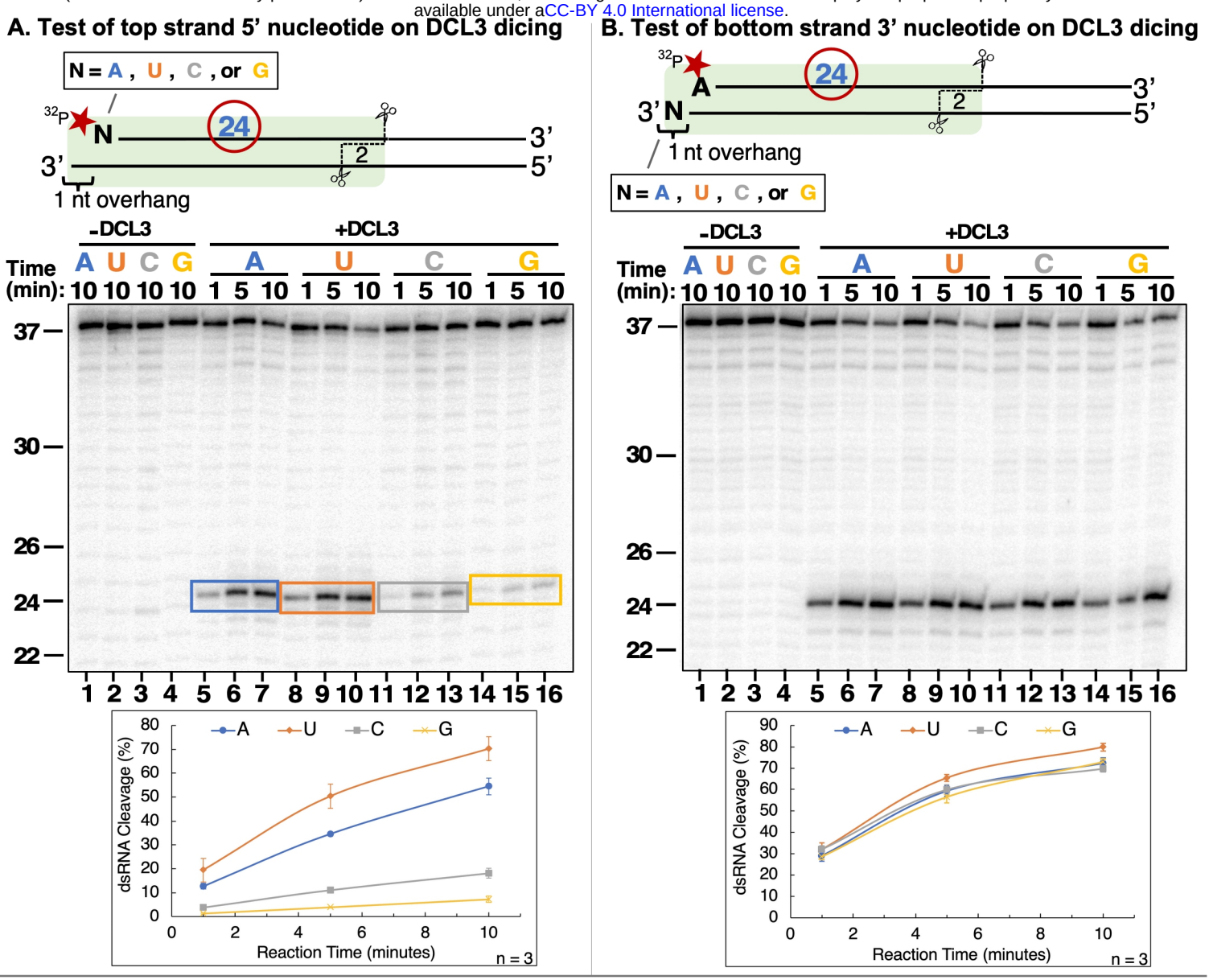

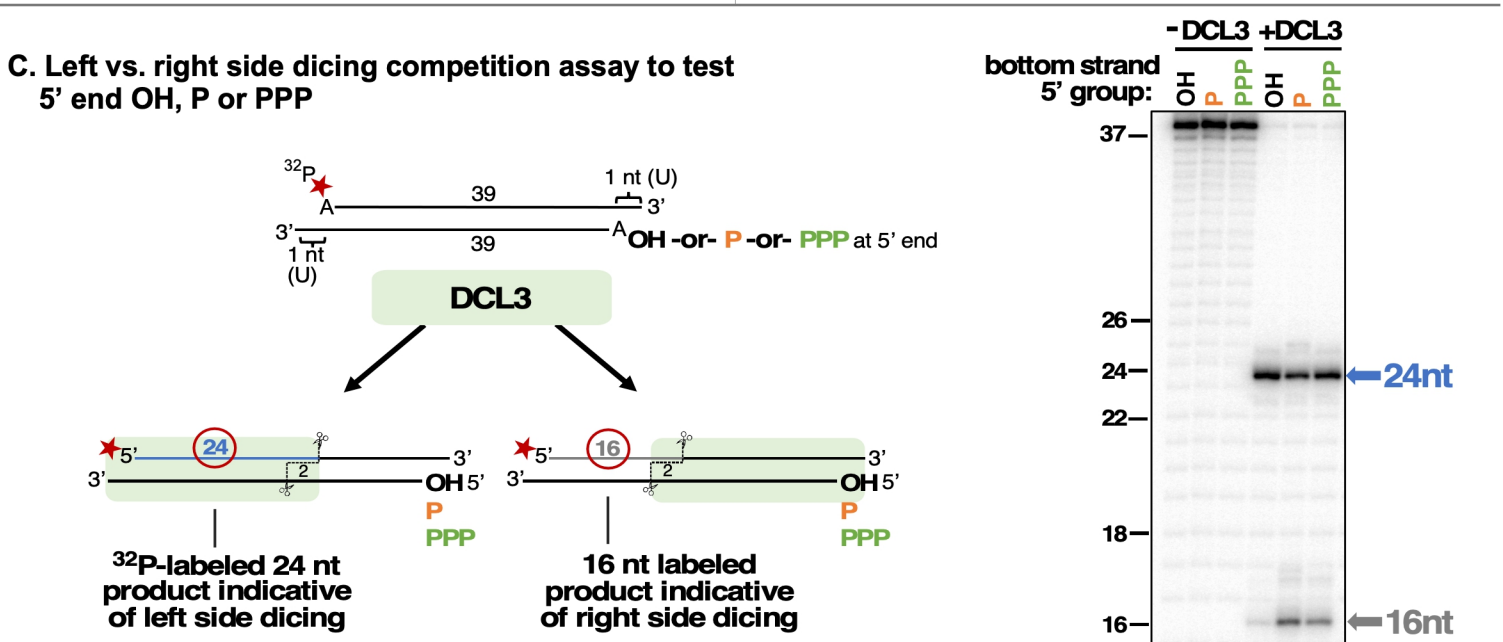

Loffer et al., Figure 4

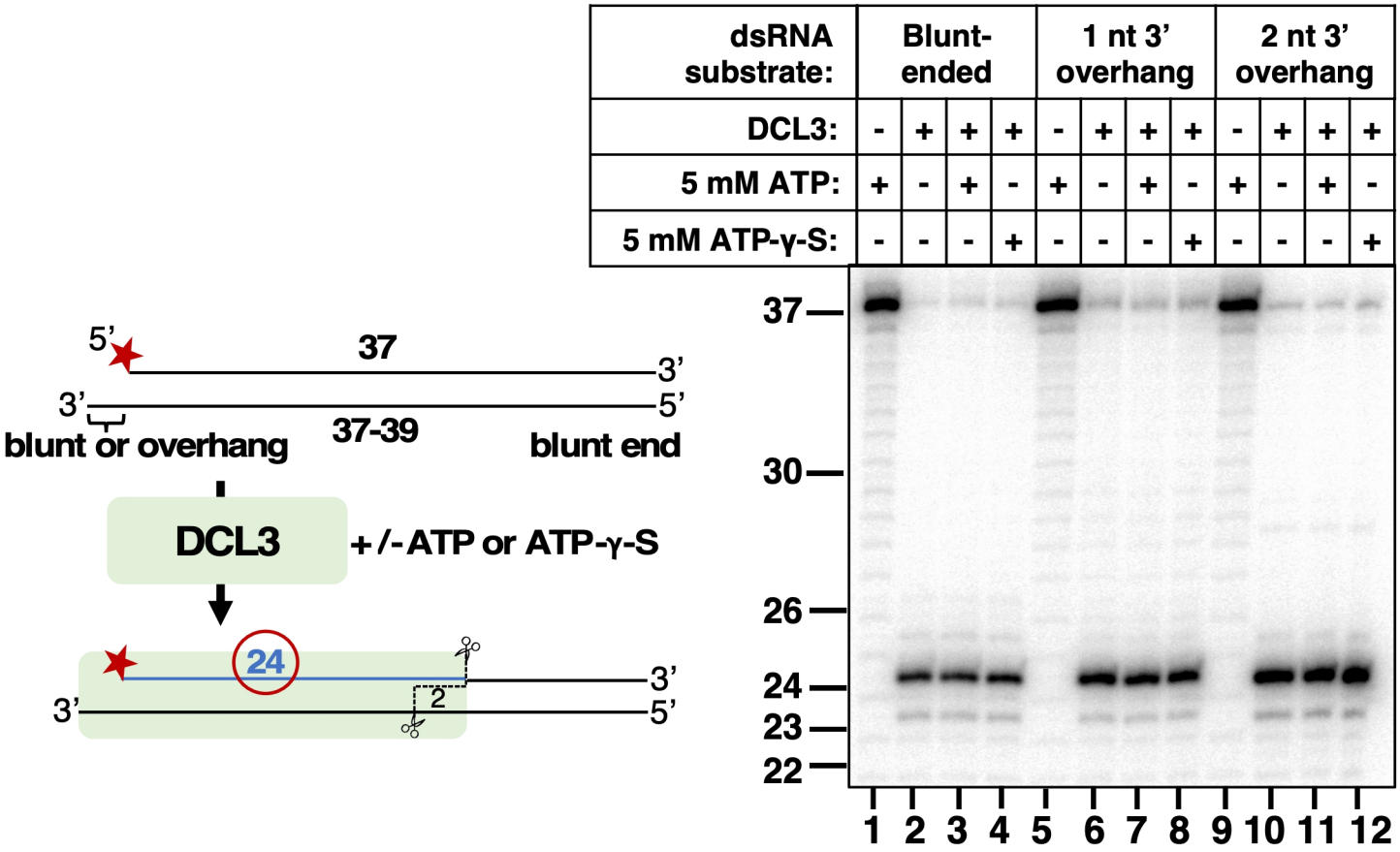

Loffer et al., Figure 5

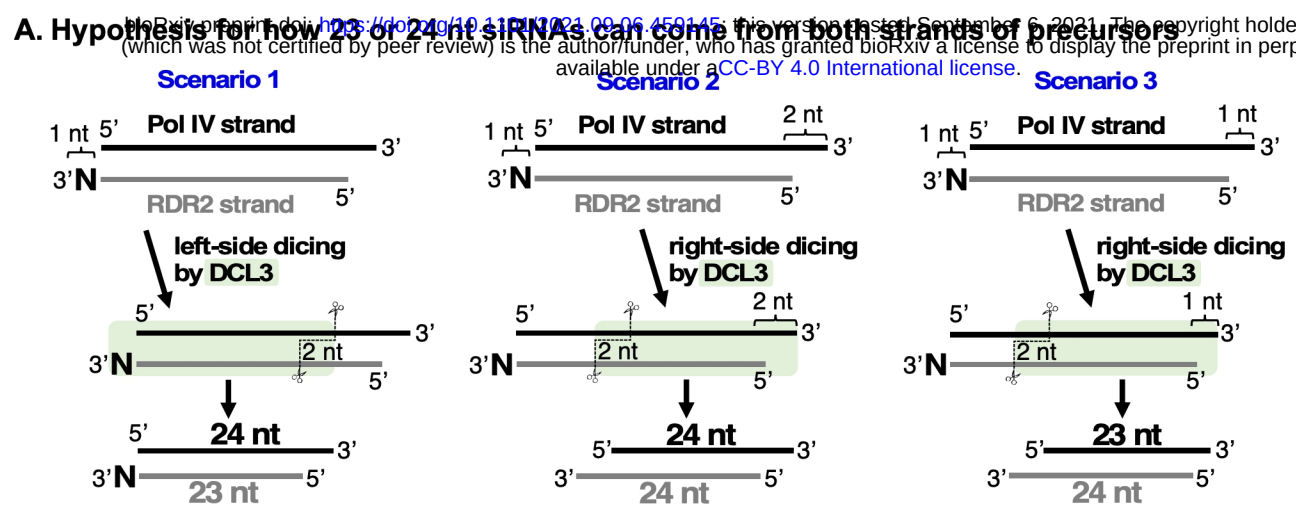

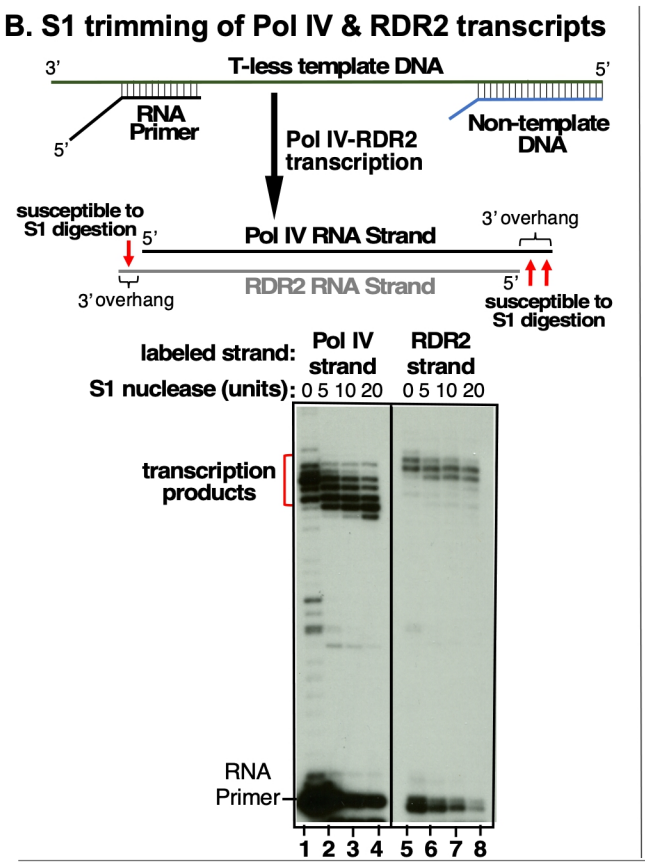

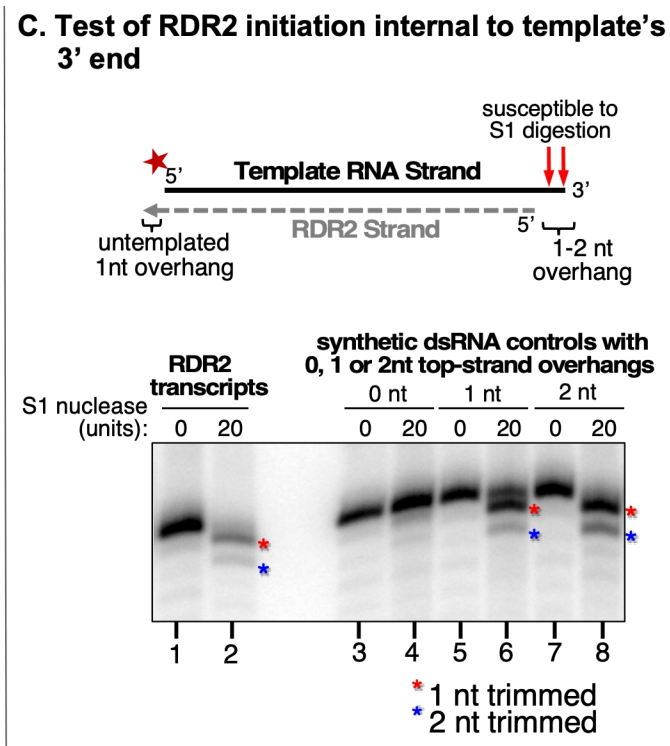

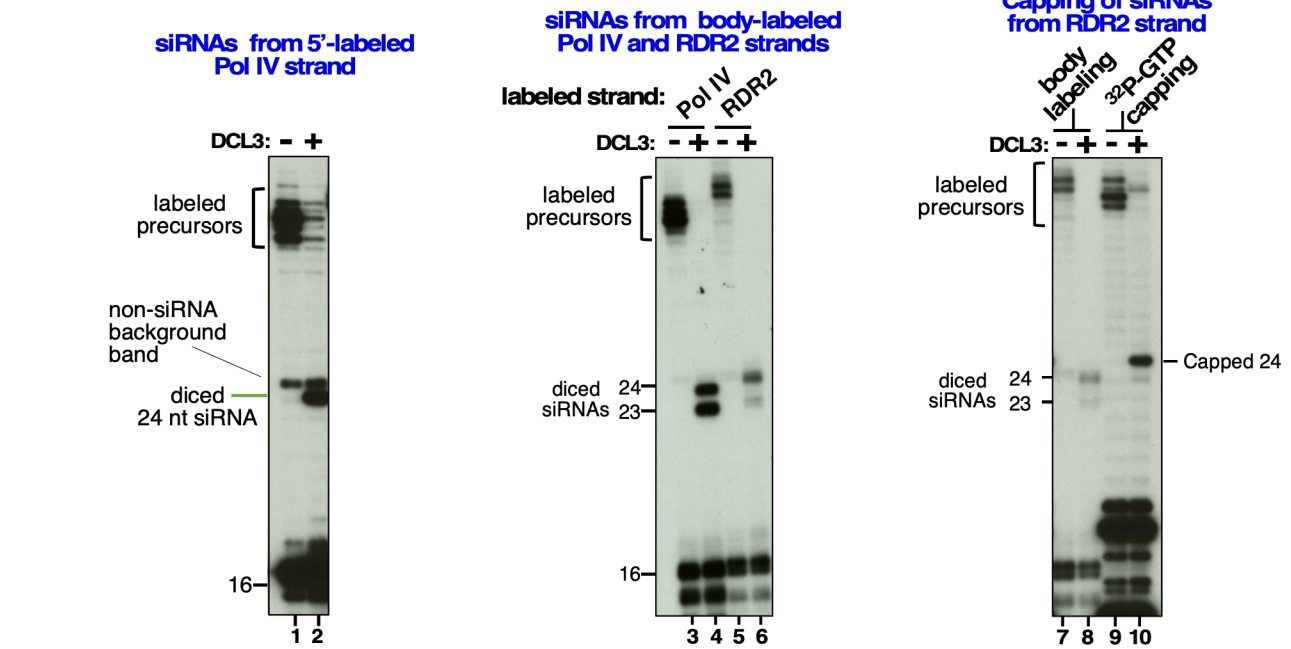

Loffer et al, Figure 6

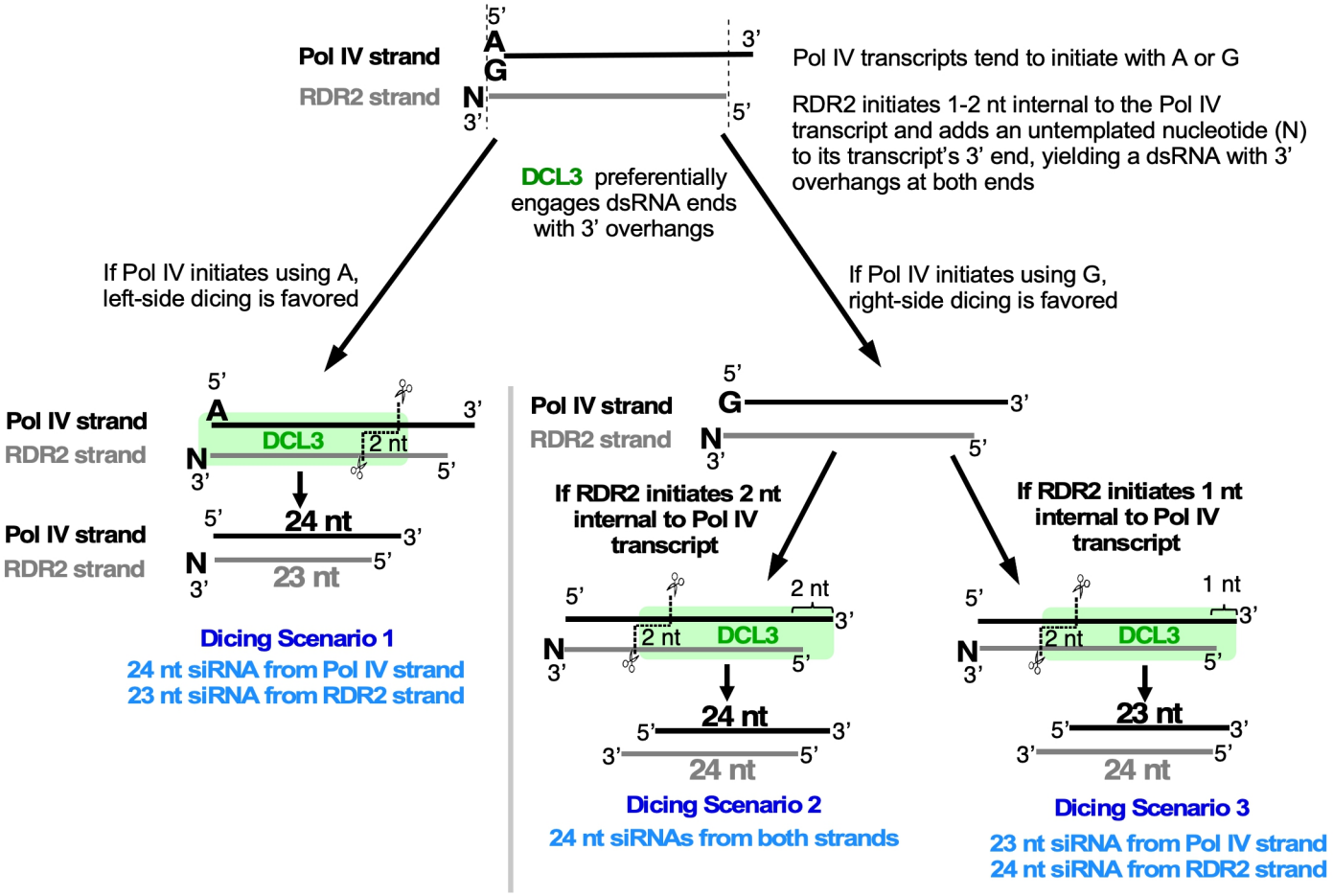

Loffer et al.
Figure 7